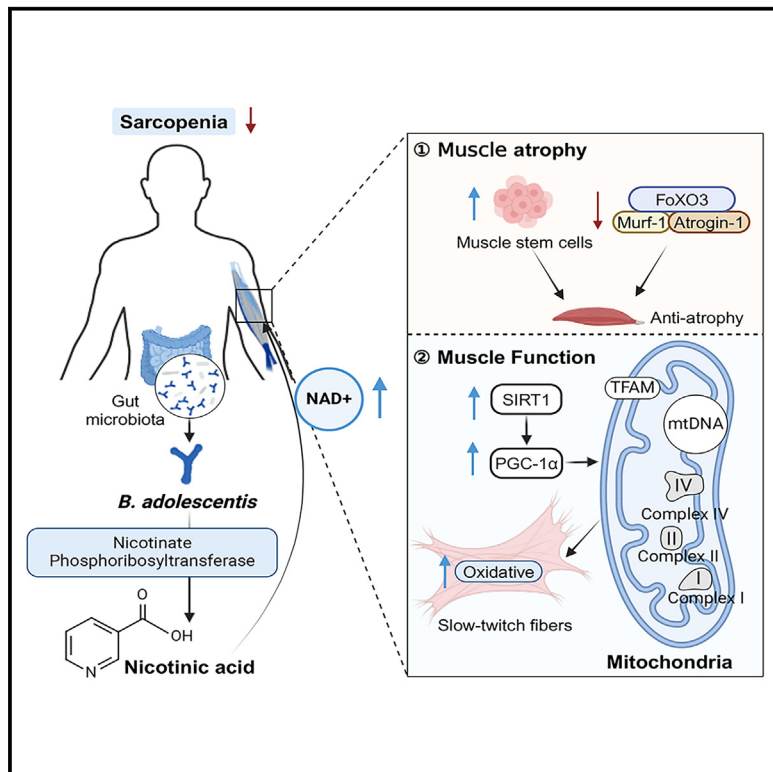


***Bifidobacterium adolescentis*-derived nicotinic acid improves host skeletal muscle mitochondrial function to ameliorate sarcopenia**

Graphical abstract



Authors

Zeng Zhang (张增), Quan Guo (郭权), Zhihan Yang (杨芷晗), ..., Yangli He, Jiahe Li, Jiachao Zhang (张家超)

Correspondence

jiachao@hainanu.edu.cn

In brief

Zhang et al. demonstrated that nicotinic acid derived from *Bifidobacterium adolescentis* increases oxidative muscle fibers in skeletal muscle and improves muscle health in individuals with sarcopenia by enhancing NAD⁺ levels, activating SIRT1/PGC-1 α , and promoting mitochondrial biogenesis.

Highlights

- Depleted *B. adolescentis* correlates with lower skeletal muscle health in sarcopenia
- *B. adolescentis*-derived nicotinic acid improves muscle mass and inhibits atrophy
- *B. adolescentis*-derived nicotinic acid boosts mitochondrial biogenesis
- NAD⁺ enhances skeletal muscle oxidative metabolism via the SIRT1/PGC-1 α axis



Article

Bifidobacterium adolescentis-derived nicotinic acid improves host skeletal muscle mitochondrial function to ameliorate sarcopenia

Zeng Zhang (张增)^{1,4} Quan Guo (郭权)^{1,4} Zhihan Yang (杨芷晗)^{1,4} Yukai Sun,¹ Shuaiming Jiang,¹ Yangli He,³ Jiahe Li,¹ and Jiachao Zhang (张家超)^{1,2,5,*}

¹School of Food Science and Engineering, Key Laboratory of Food Nutrition and Functional Food of Hainan Province, Hainan University, Haikou 570228, Hainan, China

²Collaborative Innovation Center of One Health, Hainan University, Haikou 570228, Hainan, China

³Department of Health Center, Hainan General Hospital, Hainan Affiliated Hospital of Hainan Medical University, Haikou 570311, Hainan, China

⁴These authors contributed equally

⁵Lead contact

*Correspondence: jiachao@hainanu.edu.cn

<https://doi.org/10.1016/j.celrep.2025.115265>

SUMMARY

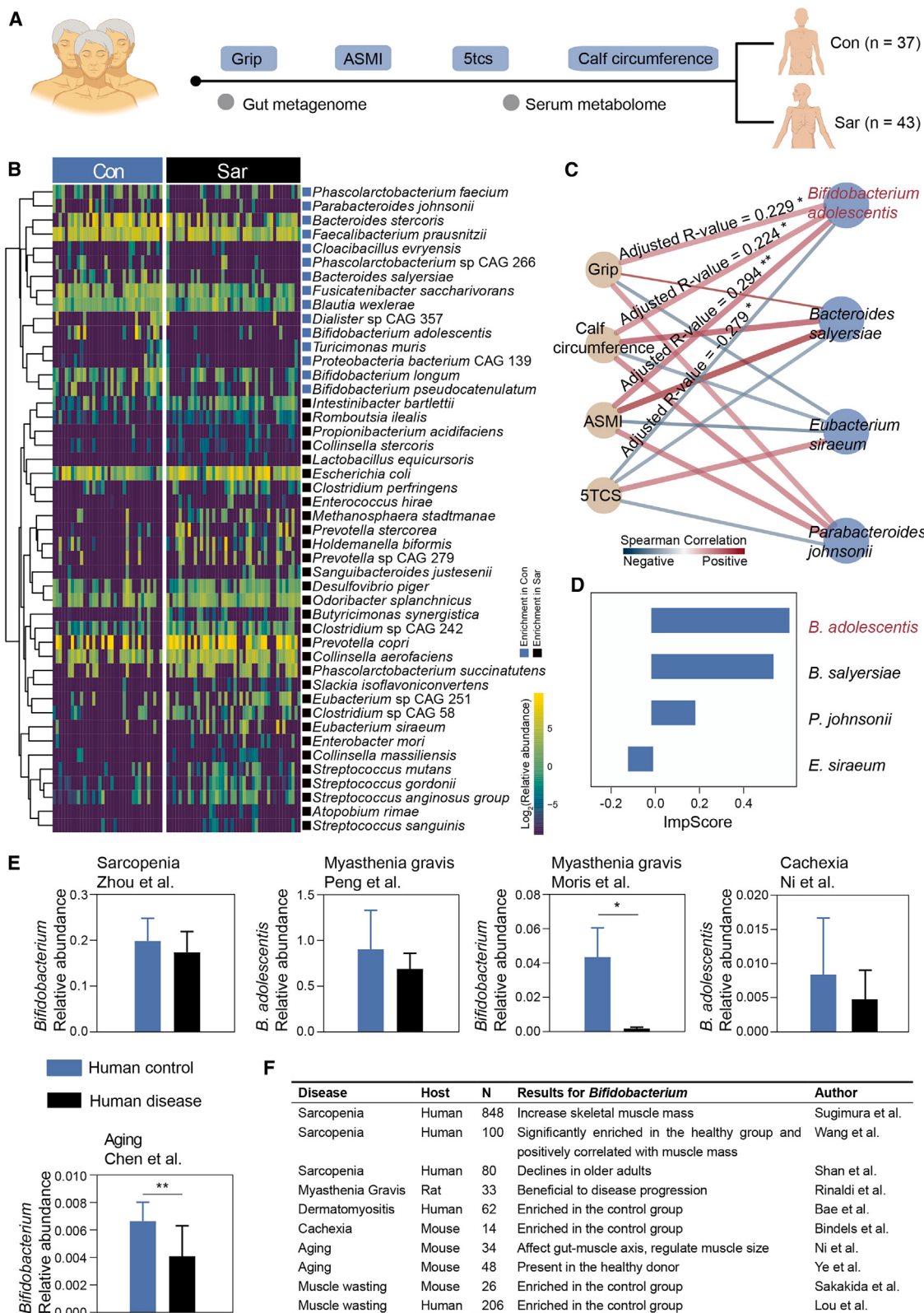
Sarcopenia significantly diminishes quality of life and increases mortality risk in older adults. While the connection between the gut microbiome and muscle health is recognized, the underlying mechanisms are poorly understood. In this study, shotgun metagenomics revealed that *Bifidobacterium adolescentis* is notably depleted in individuals with sarcopenia, correlating with reduced muscle mass and function. This finding was validated in aged mice. Metabolomics analysis identified nicotinic acid as a key metabolite produced by *B. adolescentis*, linked to improvements in muscle mass and functionality in individuals with sarcopenia. Mechanistically, nicotinic acid restores nicotinamide adenine dinucleotide (NAD⁺) levels in muscle, inhibits the FoxO3/Atrogin-1/Murf-1 axis, and promotes satellite cell proliferation, reducing muscle atrophy. Additionally, NAD⁺ activation enhances the silent-information-regulator 1 (SIRT1)/peroxisome-proliferator-activated-receptor-γ-coactivator 1-alpha (PGC-1α) axis, stimulating mitochondrial biogenesis and promoting oxidative metabolism in slow-twitch fibers, ultimately improving muscle function. Our findings suggest that *B. adolescentis*-derived nicotinic acid could be a promising therapeutic strategy for individuals with sarcopenia.

INTRODUCTION

Sarcopenia, characterized by an age-related decline in skeletal muscle mass and function, severely impacts the life quality and independence of older adults.¹ This condition raises the risk of frailty and disability, imposing a substantial economic burden on global healthcare systems.² There is sufficient evidence that sarcopenia is a significant predictor of mortality in older adults and significantly increases the risk of all-cause mortality.^{3,4} Despite extensive research efforts to understand and mitigate sarcopenia, effective therapeutic strategies remain limited. Therefore, exploring novel therapeutic approaches to address this growing health challenge is imperative. Recent research underscores the significant role of the gut microbiome in regulating host metabolism,⁵ immune function,⁶ and neurological function.⁷ Notably, aging is associated with a marked decline in gut microbiome diversity.⁸ These findings lay the groundwork for understanding the complex interactions between the gut microbiome and diseases, including sarcopenia. The concept of the gut-muscle axis

highlights that specific gut microbiota are associated with host muscle mass and strength. Studies have demonstrated that germ-free mice exhibit skeletal muscle atrophy with impaired neuromuscular junction formation.⁹ Dysbiosis of the gut microbiome may affect skeletal muscle through various pathways.¹⁰ Impaired gut barrier function due to dysbiosis can lead to systemic chronic inflammation, disrupting the balance between muscle synthesis and degradation.^{11,12} Additionally, gut microbial metabolites, such as short-chain fatty acids, regulate muscle satellite cell homeostasis,¹³ while indoxyl sulfate accelerates muscle atrophy by increasing oxidative stress and the expression of muscle atrophy genes.¹⁴ These insights suggest that the gut microbiome could be a potential therapeutic target for sarcopenia. For example, *Lactobacillus casei* Shirota has been shown to mitigate age-related muscle mass loss and strength decline by modulating the gut microbiota.¹⁵ Similarly, oral administration of *Prevotella copri* has been found to elevate blood branched-chain amino acid (BCAA) levels in mice, improve muscle function, and increase muscle mass, potentially alleviating





(legend on next page)

sarcopenia.¹⁶ Despite the promising potential of targeting the gut microbiome for sarcopenia treatment, the specific species involved and their precise mechanisms of action on muscle health remain largely unexplored. This knowledge gap hinders the development of targeted microbiome-based therapies for sarcopenia.

To address this challenge, we conducted shotgun metagenomics and metabolomics analyses on individuals with sarcopenia and matched healthy individuals. Our findings revealed a significant reduction of *Bifidobacterium adolescentis* in individuals with sarcopenia, which is closely associated with host muscle health. Using multi-omics techniques and *in vivo* validations, we elucidated the mechanism by which *B. adolescentis* improves muscle mass and function by producing nicotinic acid (NA). These findings provide new directions for developing gut-microbiome-based intervention strategies.

RESULTS

Low abundance of *B. adolescentis* correlates with reduced skeletal muscle mass and function in individuals with sarcopenia

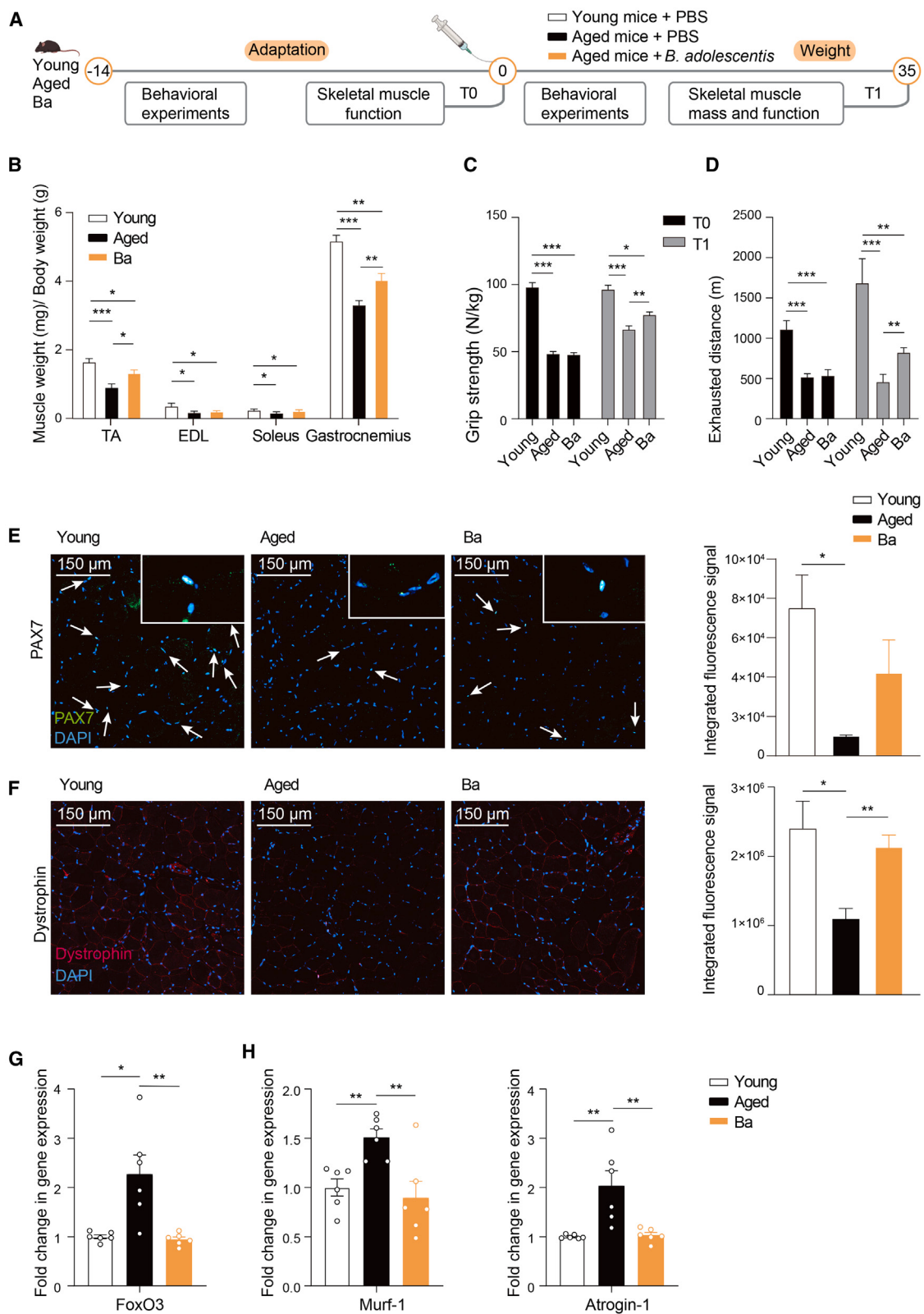
To examine associations between the gut microbiome and sarcopenia in older adults, we collected data from 43 individuals with sarcopenia (Sar group, mean age: 76.1 ± 5.9 years, 69.77% female) and 37 healthy individuals with normal muscle mass and function (Con group, mean age: 70.0 ± 4.7 years, 59.46% female). All subjects were free from medications, foods, and comorbidities known to affect the gut microbiota. Measurements of various muscle function indicators revealed that individuals with sarcopenia had a significantly lower appendicular skeletal muscle mass index (ASMI; appendicular skeletal muscle mass divided by height squared), grip strength, calf circumference, and 5-time chair stand (5TCS) compared to healthy individuals (Figures 1A and S1A).

To further understand differences in the gut microbiome, we conducted shotgun metagenomic sequencing of fecal samples from 80 subjects. For species richness, there was no significant difference in the alpha diversity of microbiome in the Con and Sar groups (Figure S1B). However, Bray-Curtis distance analysis revealed distinct gut microbiome structures between individuals with sarcopenia and healthy individuals (Adonis test, $p < 0.05$) (Figure S1C). Further analysis identified specific gut microbes affecting skeletal muscle. Both individuals with sarcopenia and

healthy individuals had the highest abundance (top 10 genus of abundance) of *Bacteroides*, followed by *Prevotella*, *Eubacterium*, and *Roseburia* (Figure S1D). However, *Bifidobacterium* and *Collinsella* were specifically enriched in the healthy individuals and individuals with sarcopenia, respectively. Differential species screening revealed that beneficial bacteria such as *Bifidobacterium longum*, *Bifidobacterium pseudocatenulatum*, and *B. adolescentis* were significantly depleted in individuals with sarcopenia (Figure 1B). These beneficial species have been extensively documented for their roles in regulating gut microbiota balance and improving host health.^{17–19} Conversely, non-beneficial species such as *Escherichia coli*, which are more abundant in patients with inflammatory bowel disease, are associated with increased inflammation and reduced muscle mass.²⁰ Among these differential species, only *B. adolescentis*, *Bacteroides salyersiae*, *Eubacterium siraeum*, and *Parabacteroides johnsonii* showed significant correlations with ASMI, grip strength, calf circumference, and 5TCS (Figure 1C). Using linear regression models to adjust for age effects, we performed Spearman correlation analyses on the adjusted residuals (representing true values excluding age factors). The results indicated that only *B. adolescentis* correlated significantly with all four indicators. Notably, a random forest model could distinguish individuals with sarcopenia from healthy individuals, with *B. adolescentis* being the most contributory species (Figure 1D). We further analyzed an additional 449 gut microbiome sequencing samples from other studies on sarcopenia and muscle-related diseases (myasthenia gravis, cachexia, and aging) to substantiate our hypothesis ($n = 60$, Zhou et al.²¹; $n = 119$, Peng et al.²²; $n = 20$, Moris et al.²³; $n = 31$, Ni et al.²⁴; and $n = 166$, Chen et al.²⁵). The abundance of *B. adolescentis* or *Bifidobacterium* has also been found to be decreased in individuals with sarcopenia or other muscle-related disease (Figure 1E). Moreover, some studies on sarcopenia have directly indicated that *Bifidobacterium* is positively correlated with host skeletal muscle mass and contributes to its increase ($n = 848$, Sugimura et al.²⁶; $n = 100$, Wang et al.²⁷; and $n = 80$, Shan et al.²⁸) (Figure 1F). In various reported clinical and animal studies on other muscle-related diseases, *Bifidobacterium* is commonly found to be enriched in the Con groups (Rinaldi et al.,²⁹ Bae et al.,³⁰ Bindels et al.,³¹ Ni et al.,³² Ye et al.,³³ Sakakida et al.,³⁴ and Lou et al.³⁵). These results indicate that the enrichment of *B. adolescentis* could be essential for preserving skeletal muscle mass and functionality in individuals with sarcopenia.

Figure 1. *B. adolescentis* are depleted in sarcopenia and significantly negatively correlated with skeletal muscle mass

- (A) Experimental strategy for multi-omics screening of gut microbiome biomarkers affecting skeletal muscle in sarcopenia.
 - (B) Comparison of differential species in the gut of the sarcopenic group (Sar group) and the healthy population (Con group). The depth of color represents the relative abundance of the species (yellow represents high abundance and blue represents low abundance, Mann-Whitney U test). Differential species were ranked based on hierarchical clustering analysis. A color block was added next to each species: the black color block indicates that the species' abundance was significantly higher in the Sar group, while the blue color block indicates that the species' abundance was significantly higher in the Con group.
 - (C) Key species significantly correlated with ASMI, grip strength, calf circumference, and 5-time sit-to-stand test. The edge color (red: positive correlation; blue: negative correlation) is proportional to the strength of the Spearman correlation. The adjusted R value represents the adjusted Spearman correlation coefficient. The * indicates that the adjusted correlation remains significant.
 - (D) Contribution of the four key species to classify subjects with or without sarcopenia.
 - (E) Relative abundance of *Bifidobacterium* or *B. adolescentis* in subjects with or without disease in other cohorts of sarcopenia or muscle-related diseases (myasthenia gravis, cachexia, and aging; Wilcoxon test).
 - (F) Results reported on *Bifidobacterium* in other published clinical or animal studies on sarcopenia or muscle-related diseases.
- Data are represented as mean \pm SEM. * $p < 0.05$, ** $p < 0.01$, and *** $p < 0.001$.



(legend on next page)

Supplementation with *B. adolescentis* significantly improves skeletal muscle mass and function in aged mice

To verify the beneficial effects of *B. adolescentis* on skeletal muscle in aged mice, we conducted a study using an aged mouse model, with young mice serving as controls (Figure 2A). The *B. adolescentis* group received daily oral administration of *B. adolescentis*, while the young and aged groups were administered an equal volume of sterile PBS daily. Oral administration of *B. adolescentis* did not significantly change the body weight of aged mice, although aged mice consistently weighed more than young mice (Figure S2A). However, the epididymal white adipose tissue (eWAT) weight was notably higher in aged mice than in young mice but significantly lower in the *B. adolescentis* group (Figure S2B). Importantly, supplementation with *B. adolescentis* significantly increased the weight of the tibialis anterior (TA), gastrocnemius, soleus, and extensor digitorum longus (EDL) muscles in aged mice (normalized to body weight), indicating a positive impact on skeletal muscle mass (Figure 2B). Further functional tests showed that *B. adolescentis* significantly enhanced the grip strength (normalized to body weight) and maximum running distance of aged mice (Figures 2C and 2D). To explore how *B. adolescentis* promotes skeletal muscle improvement, we performed paired box protein Pax-7 (PAX7) immunofluorescence staining. PAX7 is a known marker of muscle stem cells (MUSCs), crucial for skeletal muscle growth and regeneration.³⁶ Staining results showed that supplementation with *B. adolescentis* significantly enhanced PAX7-positive expression in the skeletal muscle of aged mice (Figure 2E), suggesting that *B. adolescentis* may promote muscle regeneration and repair by increasing the number of mouse MUSCs. Moreover, *B. adolescentis* intake markedly stimulated the production of dystrophin-positive muscle fibers (Figure 2F). Dystrophin is crucial for muscle membrane integrity and stability, with age-related changes in its levels impacting neuromuscular junction stability.³⁷ Further analysis showed a significant reduction in FoxO3 expression in the TA muscle of the *B. adolescentis* group compared to the aged group (Figure 2G). FoxO3, a transcription factor, regulates Atrogin-1 and Murf-1, both crucial in muscle atrophy.^{38,39} We observed a significant decrease in Atrogin-1 and Murf-1 expression in the *B. adolescentis* group (Figure 2H). Consistent patterns were found in the soleus and EDL muscles, where the expression of FoxO3, Atrogin-1, and

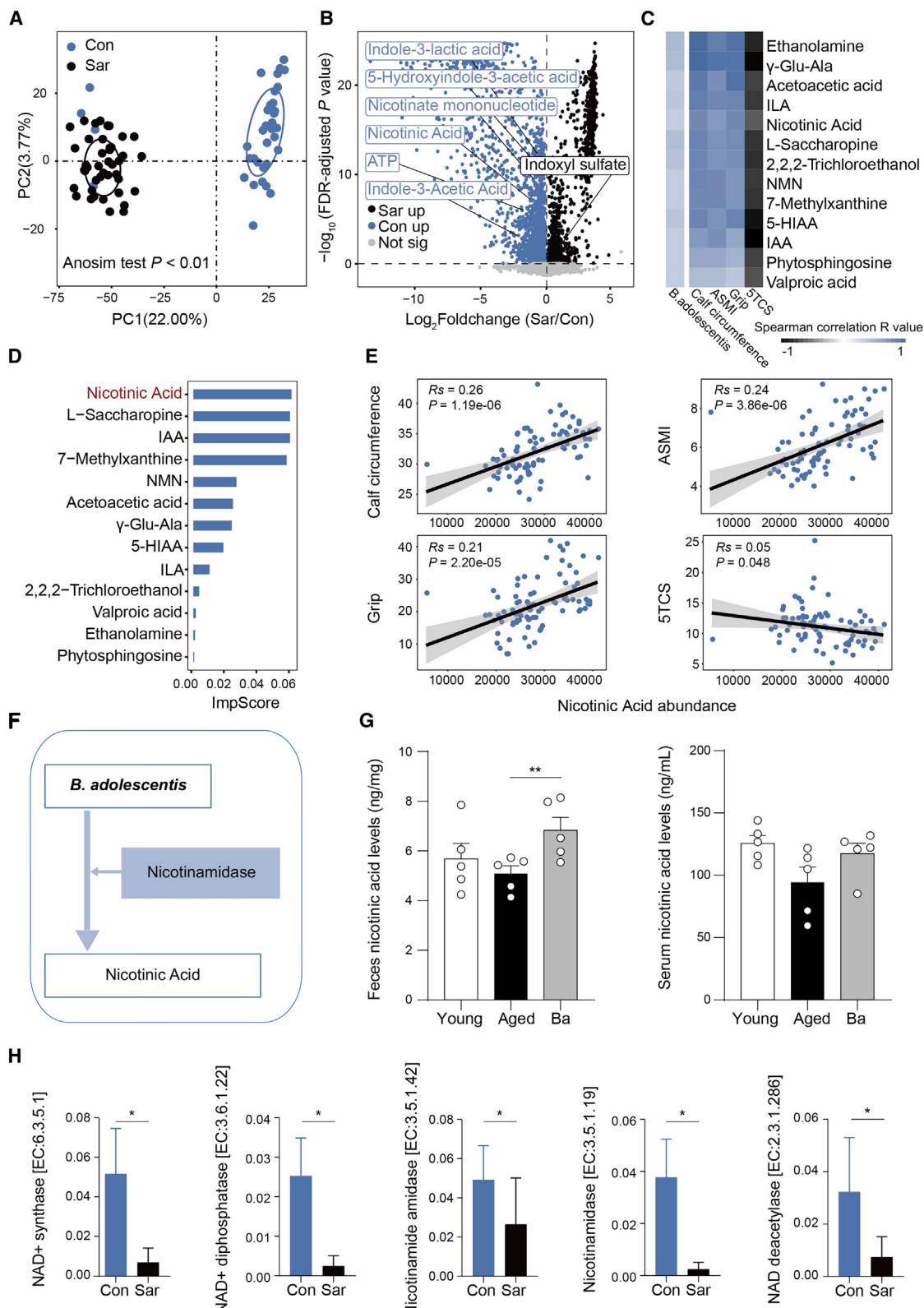
Murf-1 was significantly lower in the *B. adolescentis* group, showing no significant difference compared to the young group (Figures S2C–S2E). These results suggest that *B. adolescentis* inhibits the muscle atrophy process by downregulating FoxO3 and its downstream targets, Atrogin-1 and Murf-1. In conclusion, supplementation with *B. adolescentis* significantly improves the skeletal muscle mass and functionality in aged mice.

NA is a crucial microbial product linking *B. adolescentis* to improved skeletal muscle mass and function

To elucidate the mechanisms by which *B. adolescentis* enhances host skeletal muscle, we performed an extensive multi-omics analysis of the metagenome and metabolome in individuals with sarcopenia. Our results revealed a distinct serum metabolomic profile in individuals with sarcopenia compared to healthy individuals (analysis of similarities, Anosim test, $p < 0.01$) (Figure 3A). Several beneficial metabolites, including nicotinate mononucleotide (NMN), indole-3-lactic acid (ILA), indole-3-acetic acid (IAA), and NA were significantly reduced in individuals with sarcopenia (false discovery rate [FDR]-adjusted $p < 0.01$) (Figure 3B). Previous studies have shown that the reduction of ILA and IAA may be closely associated with age-related cognitive dysfunction, mood disorders, and muscle atrophy.⁴⁰ NA and NMN are precursors for nicotinamide adenine dinucleotide (NAD+), crucial for energy metabolism.⁴¹ Additionally, the uremic toxin indoxyl sulfate, significantly enriched in the serum of individuals with sarcopenia, induces proteolysis in muscle cells, promoting muscle atrophy.^{42,43} In addition, we observed a significant decrease in various gut-derived metabolites in individuals with sarcopenia. For example, the reduction in L-isoleucine, a key BCAA, may impact muscle protein synthesis and maintenance, thereby accelerating muscle mass loss.⁴⁴ The decrease in spermidine levels may impair muscle regeneration and function.^{45,46} Furthermore, the reduction in vitamin D is associated with weakness in type II muscle fibers, and vitamin D supplementation has been shown to have a positive effect on skeletal muscle health.⁴⁷ The decrease in γ -aminobutyric acid (GABA) may negatively affect muscle protein synthesis and degradation by inhibiting the PI3K/Akt pathway.⁴⁸ These significant changes in gut-derived metabolites suggest that multiple gut metabolites may influence skeletal muscle health through independent or synergistic mechanisms. Enrichment analysis of differential metabolites using MetaboAnalyst

Figure 2. *B. adolescentis* supplementation improves skeletal muscle mass and function in aged mice

- (A) Experimental design flowchart for *B. adolescentis* supplementation in animals.
 - (B) Weight of soleus, gastrocnemius, tibialis anterior (TA), quadriceps, and extensor digitorum longus (EDL) muscles in young and aged mice after *B. adolescentis* supplementation ($n = 8$ mice per group, Wilcoxon test).
 - (C) Grip strength (normalized to body weight) in young and aged mice before (T0) and after (T1) *B. adolescentis* supplementation ($n = 8$ mice per group, Wilcoxon test).
 - (D) Maximum running distance in young and aged mice at T0 and T1 ($n = 8$ mice per group, Wilcoxon test).
 - (E) Representative images of PAX7 immunostaining in the TA muscle (green). Arrows point to PAX7-positive cells. DAPI, 4',6-diamidino-2-phenylindole (blue, representing nuclei). Immunostaining: scale bar, 150 μ m; magnification, $\times 30$. The bar graph on the right shows the integrated fluorescence signal of PAX7 immunofluorescence for each group. t test.
 - (F) Representative images of dystrophin immunostaining in the TA muscle (red). Immunostaining: scale bar, 150 μ m; magnification, $\times 25$. The bar graph on the right shows the integrated fluorescence signal of dystrophin immunofluorescence for each group. t test.
 - (G) Changes in FoxO3 gene expression in the TA muscle among different groups ($n = 6$ mice per group, Wilcoxon test).
 - (H) Murf-1 and Atrogin-1 gene expression changes in the TA muscle among different groups ($n = 6$ mice per group, Wilcoxon test).
- Data are represented as mean \pm SEM. * $p < 0.05$, ** $p < 0.01$, and *** $p < 0.001$.



(legend on next page)

highlighted significant pathways, including vitamin B6 metabolism, arginine biosynthesis, tyrosine metabolism, tryptophan metabolism, NA and nicotinamide metabolism, and steroid hormone biosynthesis (Figure S2F). Correlation analysis indicated that only thirteen differential metabolites were significantly positively correlated with *B. adolescentis* and simultaneously significantly correlated with four muscle indicators (ASMI, grip strength, calf circumference, and 5TCS) (Figure 3C). Notably, random forest analysis identified NA as the top contributing metabolite distinguishing individuals with sarcopenia from healthy individuals (Figure 3D). Linear regression analysis further revealed significant positive correlations between NA levels and grip strength, calf circumference, ASMI, and 5TCS in individuals with sarcopenia (Figure 3E). Thus, NA emerges as a potential key metabolite through which *B. adolescentis* influences host skeletal muscle. Using the MetOrigin database and BLAST comparison of protein sequences, we identified that *B. adolescentis* produces NA via NA phosphoribosyltransferase (k00763) (Figure 3F). Subsequently, we quantified the levels of NA in the serum and feces of mice from the previous animal experiments. The supplementation with *B. adolescentis* was found to elevate NA levels in their feces and serum. The results confirmed that NA is a metabolite of *B. adolescentis* (Figure 3G). Furthermore, the gut microbiome's metagenomic functions of individuals with sarcopenia were annotated using the KEGG database. Given the focus on NA, we found that the NA and nicotinamide metabolism pathway was reduced in individuals with sarcopenia, although not significantly. Interestingly, the mitochondrial biogenesis pathway was significantly decreased in individuals with sarcopenia (Figure S2G). Further stratification of NA and nicotinamide metabolism to *B. adolescentis* revealed a reduction in five NAD+-related metabolic pathways in individuals with sarcopenia (Figure 3H). In conclusion, the high abundance of *B. adolescentis* may enhance host skeletal muscle mass and function by producing the key metabolite, NA. This effect is potentially achieved through the generation of more NAD+.

NA supplementation significantly enhanced skeletal muscle mass and function in aged mice

Having established that *B. adolescentis* enhances host skeletal muscle mass and function through NA production, we pro-

ceeded to investigate whether NA supplementation could affect skeletal muscle mass and function in aged mice (Figure 4A). Notably, aged mice receiving NA supplementation did not exhibit significant body weight changes compared to the aged group (Figure S3A). In contrast, the eWAT weight in the aged group remained significantly higher than in the young and NA groups (Figure S3B). At T0 (before the NA supplementation), grip strength (normalized to body weight) and maximum running distance in the NA group were similar to the aged group but significantly lower than the young group (Figure S3C). After 5 weeks of NA supplementation, the NA group significantly improved grip strength and maximum running distance (Figure 4B). NA supplementation also significantly increased the weight of TA, gastrocnemius, soleus, and EDL muscles in aged mice (normalized to body weight) (Figure 4C). Unsurprisingly, the levels of NA in the serum and feces of the NA group were significantly elevated and comparable to those in the young group (Figure 4D). Additionally, NA supplementation significantly reduced the relative expression levels of FoXO3, Atrogin-1, and Murf-1 in the soleus, EDL, and TA muscles of aged mice (Figures 4E, 4F and S3D–S3F). To further investigate whether NA treatment directly affects the FoXO3/Atrogin-1/Murf-1 pathway, we used an established *in vitro* myotube culture model to study the impact of NA on dexamethasone-induced muscle atrophy. The dexamethasone-induced muscle atrophy model is widely used to validate the role of the FoXO3/Atrogin-1/Murf-1 pathway.^{49–51} In the dexamethasone-treated C2C12 myotubes, the expression of FoXO3, Atrogin-1, and Murf-1 was elevated. In contrast, NA treatment significantly reduced the dexamethasone-induced upregulation of FoXO3, Atrogin-1, and Murf-1 expression (Figure 4G). Increased immunofluorescence intensity of PAX7 was observed, although it was still lower than in the young group (Figure 5A). Next, we further investigated whether NA supplementation could directly promote the proliferation of MUSCs. MUSCs were seeded in media containing NA at the same density and cultured for 48 h, resulting in a significant increase in cell number (Figure 5B). Additionally, the 5-ethynyl-2'-deoxyuridine (EdU) assay showed a significantly higher proportion of EdU-positive cells in the NA treatment group compared to the control group (Figure 5C). These findings suggest that NA significantly promotes the proliferation of MUSCs,

Figure 3. Nicotinic acid produced by *B. adolescentis* is depleted in sarcopenia and significantly negatively correlated with skeletal muscle mass

- (A) Principal-component analysis (PCA) plot of serum metabolomics in subjects. Each point represents a subject sample. The clustering of sample distribution indicates structural differences in the metabolome (Anosim test).
 - (B) Comparison of differential metabolites in the serum metabolome of subjects. Each point represents a metabolite. Blue points represent metabolites enriched in the Con group (\log_2 fold change < 0). Black points represent metabolites enriched in the Sar group (\log_2 fold change > 0). Gray points represent non-significant metabolites. Points with $-\log_{10}(\text{FDR-padjust}) > 0$ represent significant differences (FDR-padjust < 0.05). The smaller the FDR-adjusted p value, the closer the dot is to the top of the graph; the greater the abundance change, the closer the dot is to the left or right side. Student's t test.
 - (C) Key metabolites significantly correlated with *B. adolescentis* and clinical indicators (ASMI, grip strength, calf circumference, and 5TCS). The color of the cells represents the Spearman correlation coefficient (R value) between the metabolites and *B. adolescentis* or clinical indicators (ranging from –1 to 1). The darker the color, the stronger the correlation. Blue represents a positive correlation, and black represents a negative correlation.
 - (D) Contribution of 13 key species to classify subjects with or without sarcopenia.
 - (E) Linear relationship between nicotinic acid and ASMI, grip strength, calf circumference, and 5TCS.
 - (F) Schematic of nicotinic acid production by *B. adolescentis*.
 - (G) The nicotinic acid level in the feces and serum of mice with or without *B. adolescentis* gavage ($n = 5$ mice per group, Wilcoxon test).
 - (H) Metagenomic functional annotation of the gut microbiome in subjects with or without sarcopenia based on the KEGG database. Nicotinic acid metabolism further stratified to *B. adolescentis*, showing significant reductions in five NAD+-related metabolic pathways in sarcopenia (Wilcoxon test).
- Data are represented as mean \pm SEM. * $p < 0.05$, ** $p < 0.01$, and *** $p < 0.001$.

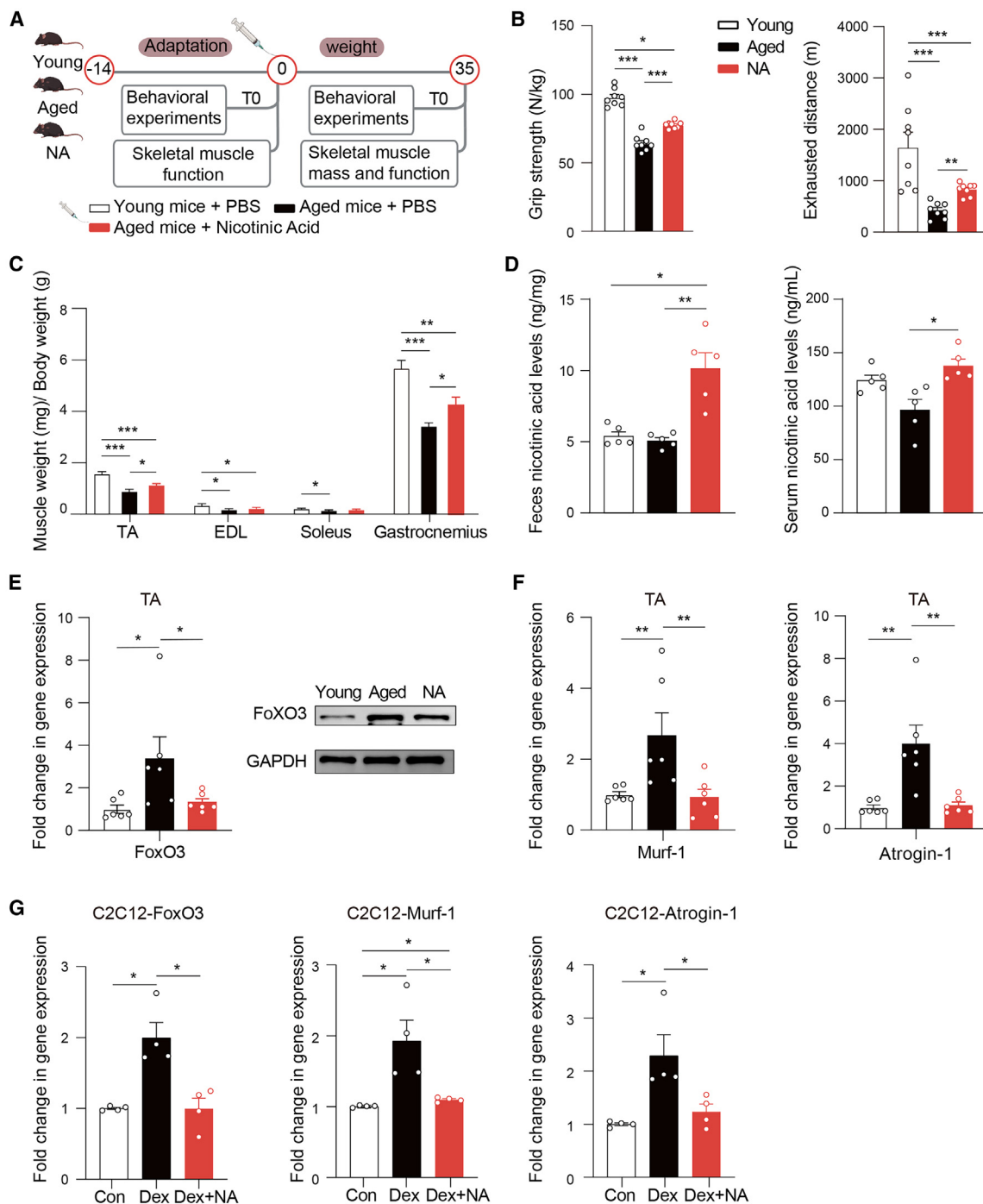


Figure 4. Nicotinic acid supplementation improves skeletal muscle mass and function in aged mice

(A) Experimental design flowchart for nicotinic acid supplementation in animals.

(B) Grip strength (normalized to body weight) and maximum running distance in young and aged mice after nicotinic acid supplementation (T1) ($n = 8$ mice per group, Wilcoxon test).

(C) Weight of soleus, gastrocnemius, TA, quadriceps, and EDL muscles in young and aged mice after nicotinic acid supplementation ($n = 8$ mice per group, Wilcoxon test).

(D) Nicotinic acid content in serum and feces of young and aged mice after nicotinic acid supplementation ($n = 6$ mice per group, Wilcoxon test).

(legend continued on next page)

which is consistent with previous studies.³⁶ Similarly, NA intake markedly stimulated the production of dystrophin-positive muscle fibers (Figure 5D). These findings further support the critical role of NA as a metabolite produced by *B. adolescentis* in enhancing host skeletal muscle mass and function.

NAD⁺ enrichment enhances mitochondrial biogenesis via PGC-1 α activation

The observed improvements in skeletal muscle function in aged mice following supplementation with both *B. adolescentis* and NA prompted us to investigate the underlying mechanisms affecting muscle mass and function. NAD⁺ is well known for its critical role in regulating mitochondrial quantity and function, and NA, a precursor of NAD⁺, can significantly elevate NAD⁺ concentrations⁵² (Figure S3G). In our study, supplementation with *B. adolescentis* and NA markedly elevated NAD⁺ levels in serum, TA, and soleus muscles, reaching levels comparable to those in the young group (Figures 6A and S4A). The increase in NAD⁺ levels was also observed in both NA-treated C2C12 cells and MUSCs (Figure S3H). Therefore, NAD⁺ supplementation can directly regulate the skeletal muscle FoXO3/Atrogin-1/Murf-1 pathway and promote the proliferation of MUSCs. Silent-information-regulator 1 (SIRT1) activity, which is highly sensitive to changes in cellular energy states and regulated by NAD⁺, subsequently activates peroxisome-proliferator-activated-receptor- γ -coactivator 1-alpha (PGC-1 α),⁵³ promoting mitochondrial biogenesis. Following supplementation with NA and *B. adolescentis*, the expression levels of SIRT1 and PGC-1 α significantly rose in the TA and soleus muscles (Figures 6B, 6C, S4B, and S4C). Earlier researches have demonstrated that PGC-1 α modulates the expression of nuclear respiratory factors 1 and 2 (NRF1 and NRF2), which subsequently regulate mitochondrial transcription factor A (Tfam).⁵⁴ Consistent with these findings, our results showed that treatment with both *B. adolescentis* and NA significantly increased the expression of NRF1 and NRF2 in TA and soleus muscles (Figures 6D, S3I, and S4D). Additionally, this pathway significantly enhanced the mitochondrial DNA content (assessed by the mtDNA/nuclear DNA ratio) and Tfam expression in the TA and soleus of the *B. adolescentis* and NA groups (Figures 6E, 6F, S4E, and S4F). Tfam plays a crucial role in mitochondrial biogenesis and mtDNA replication.⁵⁵ Moreover, *B. adolescentis* and NA treatments significantly increased citrate synthase activity in the gastrocnemius and soleus muscles, indicating an increase in skeletal muscle mitochondrial content (Figures 6G and S4G). The increased fluorescence intensity of complex IV (COX IV) staining in the TA and soleus muscles of the NA and *B. adolescentis* groups further confirmed the enhancement of mitochondrial function (Figures 6H and S4H). These results demonstrate that NA supplementation promotes mitochondrial biogenesis through NAD⁺ enrichment and PGC-1 α activation.

Enhanced oxidative metabolism and ATP production in skeletal muscle following NA treatment

The increase in mitochondrial biogenesis following NA supplementation was accompanied by significant improvements in oxidative metabolism and ATP production. NA and *B. adolescentis* significantly enhanced mitochondrial respiratory chain complex I and II activities in both TA and soleus muscles (Figures 7A and S5A), leading to elevated ATP levels in mice (Figures 7B and S5B). This result corresponded with significantly reduced ATP content observed in the serum of individuals with sarcopenia relative to healthy individuals (Figure 7C). At the cellular level, NA-treated C2C12 myoblasts exhibited a significant increase in oxygen consumption rates (OCRs), further confirming the improvement in mitochondrial oxidative function (Figure 7D). Previous studies have shown that activation of PGC-1 α can increase the expression of oxidative muscle fibers and mitochondrial genes in muscles.⁵⁶ In the soleus muscle, which is predominantly composed of slow-twitch fibers, NA and *B. adolescentis* treatment significantly increased the proportion and cross-sectional area (CSA) of slow muscle fibers (MyHC-I) (Figures 7E–7G, S5C, and S5E). This enhancement is likely due to NA activating the PGC-1 α /SIRT1 pathway via NAD⁺, which plays a critical role in improving the metabolic adaptation of slow oxidative fibers. In the TA, which is primarily composed of fast-twitch fibers, there were no significant changes in the proportion of fast muscle fibers (MyHC-IIb) following NA and *B. adolescentis* treatment, and the peak value of the fiber area frequency distribution ($300 \mu\text{m}^2$) remained unchanged. However, in the larger-area segment ($1,500 \mu\text{m}^2$), the number of fast muscle fibers in the NA-treated group was significantly higher compared to the aged control group (Figures 7F–7H, S5D, and S5F). This might be due to NAD⁺ reducing muscle atrophy by inhibiting the FoXO3/Atrogin-1/Murf-1 pathway and promoting the proliferation of skeletal MUSCs. These results suggest that while the PGC-1 α pathway primarily regulates the metabolism of slow muscle fibers, the protective effects of NA on fast muscle fibers should not be overlooked. Overall, the elevation of NAD⁺ improves MUSCs and function in aged hosts through enhanced metabolic function and anti-atrophy mechanisms.

DISCUSSION

Here, we investigated the therapeutic role of *B. adolescentis*-produced NA on sarcopenia using shotgun metagenomics and metabolomics. *B. adolescentis* was significantly depleted in the gut of sarcopenic subjects, correlating with reduced skeletal muscle strength, grip strength, and physical function. NA was identified as the key microbial effector through which *B. adolescentis* influences skeletal muscle. Supplementation with *B. adolescentis* and NA improved skeletal muscle mass and function in aged mice. Mechanistically, this supplementation increased the number of MUSCs, inhibited the expression of

(E) Changes in FoxO3 gene expression in the TA muscle among different groups ($n = 6$ mice per group, Wilcoxon test). Shown on the right are immunoblot analyses of protein lysates in the TA muscle of various groups of mice.

(F) Murf-1 and Atrogin-1 gene expression changes in the TA muscle among different groups ($n = 6$ mice per group, Wilcoxon test).

(G) FoxO3, Murf-1, and Atrogin-1 gene expression changes in the C2C12 cells among different groups. Wilcoxon test.

Data are represented as mean \pm SEM. * $p < 0.05$, ** $p < 0.01$, and *** $p < 0.001$.

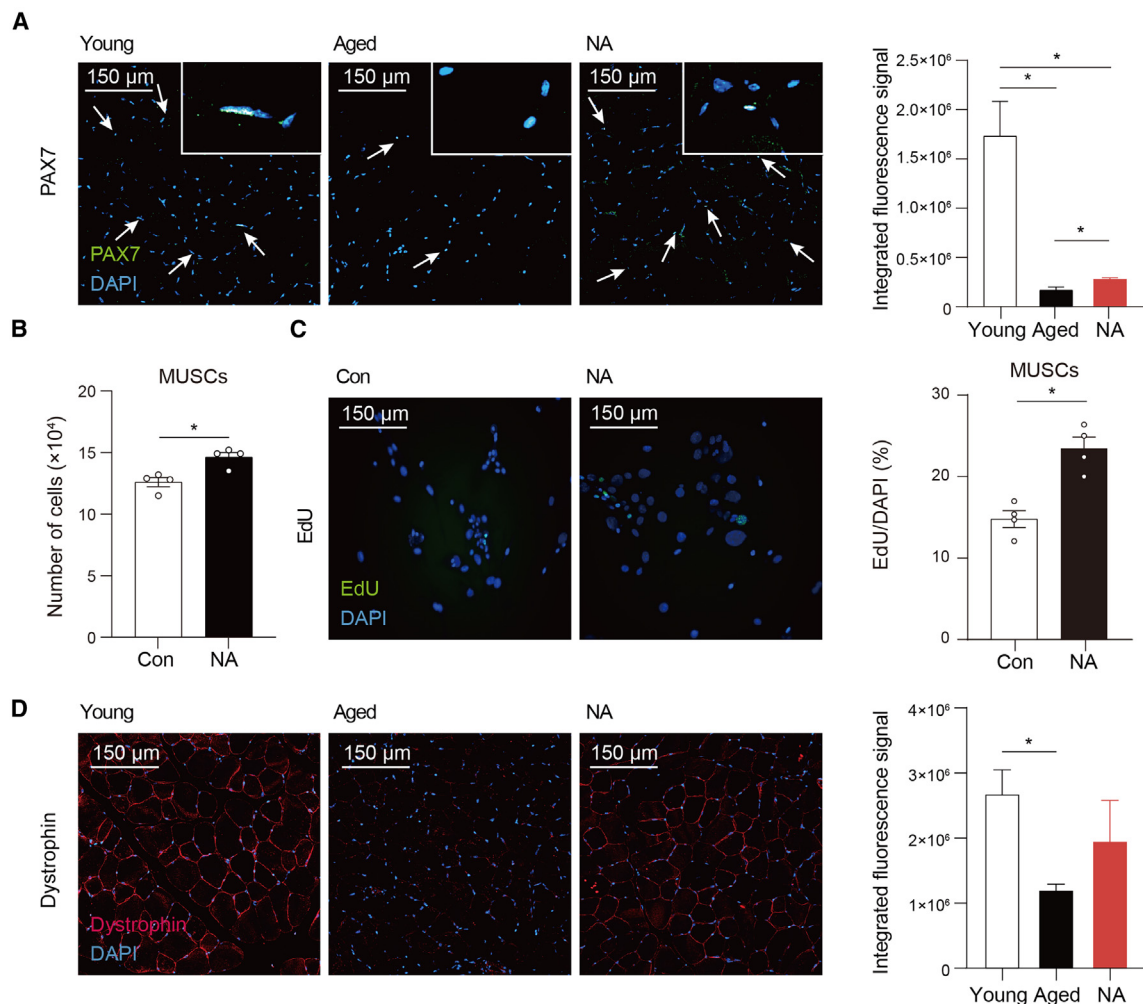
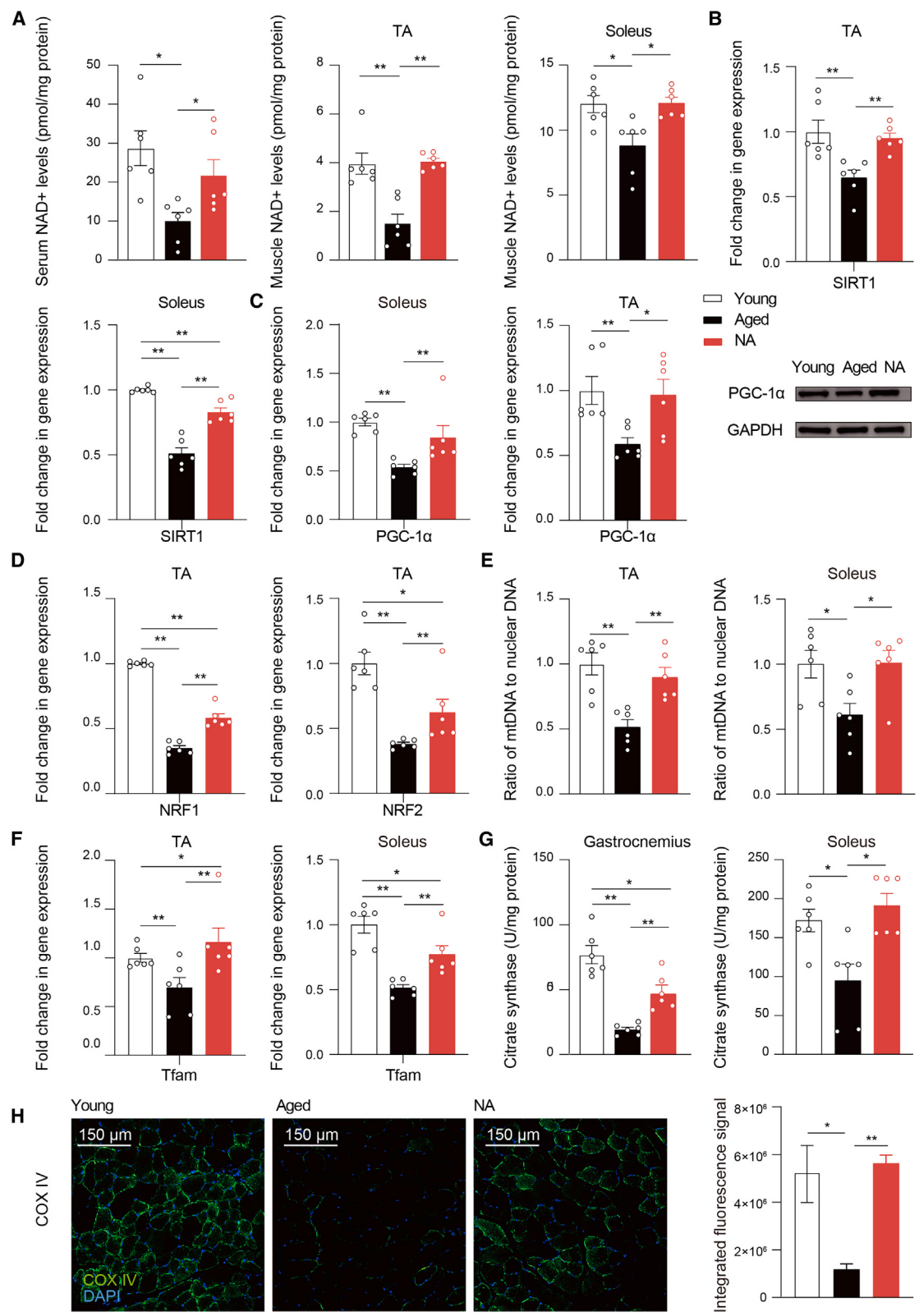


Figure 5. Nicotinic acid supplementation promotes proliferation of MUSCs

(A) Representative images of PAX7 immunostaining in the TA muscle (green). Arrows point to PAX7-positive cells. Immunostaining: scale bar, 150 μ m; magnification, $\times 30$. The bar graph on the right shows the integrated fluorescence signal of PAX7 immunofluorescence for each group. t test.
 (B) Number of cells in MUSCs in each group after nicotinic acid intervention. Wilcoxon test.
 (C) Representative images of EdU immunostaining in MUSCs (green). Immunostaining: scale bar, 150 μ m; magnification, $\times 200$. DAPI, 4',6-diamidino-2-phenylindole (blue, representing nuclei). Wilcoxon test.
 (D) Representative images of dystrophin immunostaining in the TA muscle (red). Immunostaining: scale bar, 150 μ m; magnification, $\times 25$. The bar graph on the right shows the integrated fluorescence signal of dystrophin immunofluorescence for each group. t test.
 Data are represented as mean \pm SEM. * $p < 0.05$, ** $p < 0.01$, and *** $p < 0.001$.

muscle atrophy genes, and elevated NAD⁺ levels in skeletal muscle and serum. Consequently, this activated SIRT1 upregulated PGC-1 α and enhanced the quantity and function of skeletal muscle mitochondria, leading to increased ATP content. The expression of PGC-1 α in skeletal muscle has been reported to increase oxidative muscle fibers and provide protective effects against sarcopenia.⁵⁶ Importantly, previous studies have indicated that targeting the activation of PGC-1 α expression to prevent muscle loss is a reasonable approach. Overexpression of PGC-1 α has been shown to correct the decline in antioxidant capacity and the increase in nuclear factor κ B (NF- κ B) nuclear binding associated with sarcopenia. The increase in PGC-1 α levels appears to be crucial not only for restoring common mus-

cle changes but also for the restoration of overall functional ability in aging organisms.⁵⁷ When PGC-1 α is expressed in skeletal muscle, it leads to various changes, including mitochondrial biogenesis, angiogenesis, and resistance to muscle atrophy.⁵⁸ Additionally, the elevation of PGC-1 α has been shown to suppress the severe loss of muscle mass induced by FoxO3.^{59,60} Therefore, the increase in mitochondrial content or the enhancement of oxidative metabolism driven by PGC-1 α may indirectly help prevent skeletal muscle atrophy.⁶⁰ In this study, *B. adolescentis* and NA improve host skeletal muscle function by enhancing muscle oxidative metabolism. Our current data suggest that the increase in host skeletal muscle mass may be attributed to NAD⁺ suppression of the FoxO3/Atrogin-1/Murf-1



(legend on next page)

pathway, which helps delay muscle atrophy and maintain muscle tissue quality.⁵⁰ Furthermore, the proliferative effect of NAD⁺ on skeletal MUSCs aids in muscle regeneration and helps combat muscle atrophy.^{61,62} Although we do not have sufficient data to directly link the inhibition of the FoxO3/Atrogin-1/Murf-1 pathway with the upregulation of PAX7 expression, this finding is consistent with a report that associates the FoxO3 pathway with the improvement of MUSC dysfunction.⁶³ Additionally, previous studies have shown that overexpression of FoXO3 downregulates PAX7.⁶⁴ The relationship between these two factors may be linked to oxidative stress in skeletal muscle. On the one hand, FoXO3 is activated when cellular reactive oxygen species (ROS) levels are elevated, and on the other hand, FoXO3 itself can trigger ROS accumulation.^{65–67} High levels of ROSs in skeletal muscle can inhibit MUSC function and PAX7 expression.^{68,69}

The role of the gut microbiome in older adults has attracted much attention in recent years. Evidence suggests that changes in the gut microbiome are strongly correlated with declines in skeletal muscle function.⁷⁰ Gut dysbiosis related to sarcopenia may affect muscle function through various mechanisms, including the production of metabolic products, regulation of inflammatory responses, and absorption and utilization of nutrients.⁷¹ We analyzed the gut microbiota characteristics in older adults, comparing individuals with and without sarcopenia. We found that beneficial species such as *B. adolescentis* and *B. longum* were significantly reduced in the gut of sarcopenic subjects. Research indicates that *B. longum* can enhance mitochondrial activity and increase muscle mass, improving locomotion and longevity in aging models such as *Caenorhabditis elegans*.⁷² Supplementation with *B. adolescentis*, enriched in the gut of Italian centenarians,⁷³ may extend various animal models' health span and lifespan by upregulating host catalase activity.²⁵ Using a random forest model, we further confirmed the association between the reduction of *B. adolescentis* and sarcopenia, suggesting its critical role in maintaining muscle function. Considering the importance of the gut-muscle axis in regulating muscle metabolism, this finding has significant clinical implications.⁷⁴ This result has also been validated in other cohorts and muscle-related disease cohorts. Additionally, *B. adolescentis* can alleviate constipation and dextran sulfate sodium-induced chronic colitis in mice by modulating the gut microbiota.^{75,76} This further supports the significance of gut microbiota in the health of older adults. Modulating the gut microbiome can improve skeletal muscle function through multiple pathways.⁵⁰

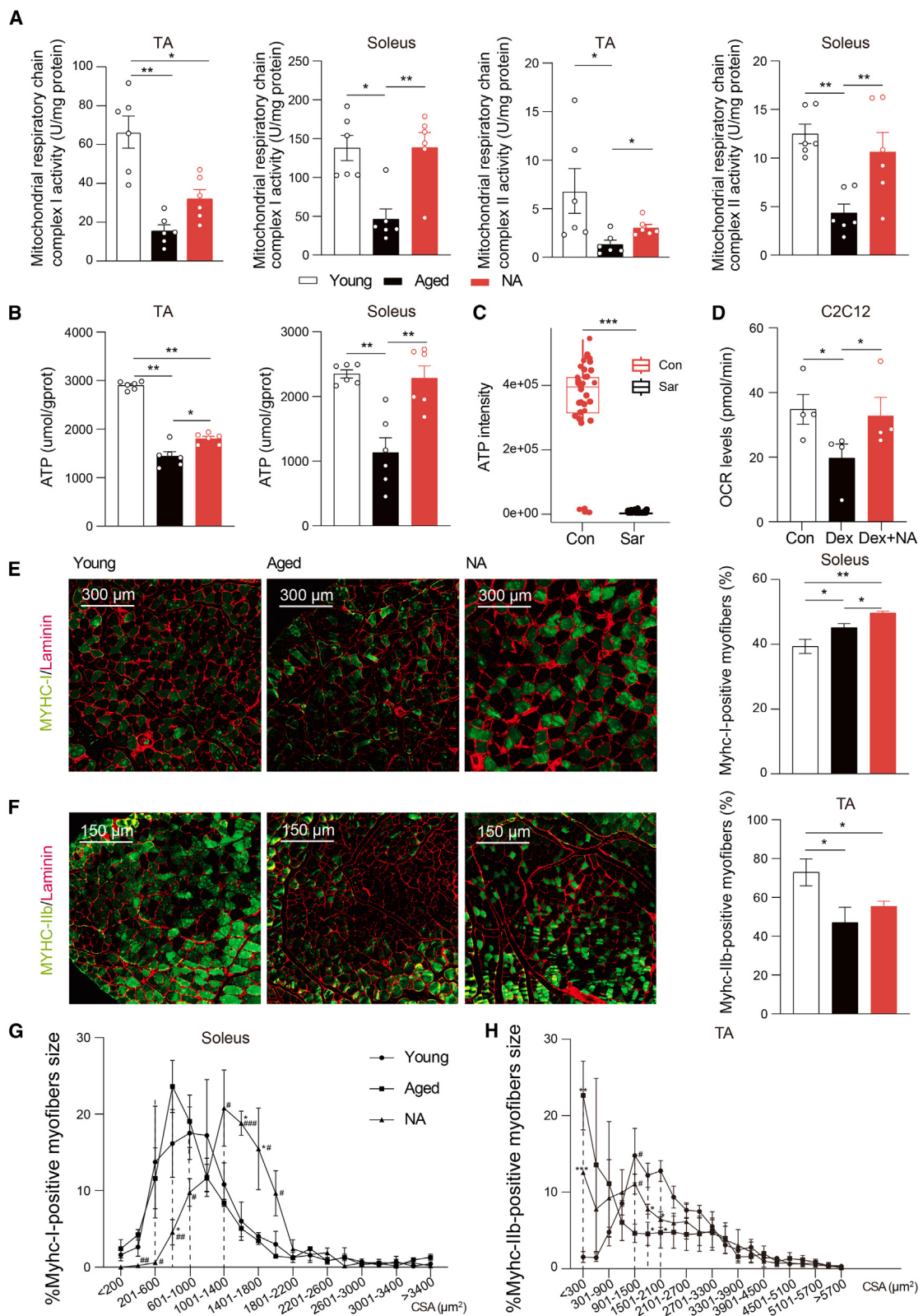
Research has shown that changes in the gut microbiome can promote muscle health by regulating host metabolism and immune responses, reducing inflammation and oxidative stress.⁷⁷

Based on multi-omics technologies, we further elucidated the relationship between the metabolic functions of the gut microbiome and sarcopenia. In addition to the reduction of some known beneficial metabolites in individuals with sarcopenia, we observed a significant decrease in serum NA levels. This serves as a crucial link between *B. adolescentis* and sarcopenia. Many bacteria can encode nicotinamidase and nicotinate phosphoribosyltransferase to synthesize NA.^{78,79} Even without dietary NA, microbial production of NA remains sufficiently high to maintain host circulating levels.^{80,81} As previously reported, a high NA diet resulted in altered skeletal muscle fibers and improved endurance in mice.⁸² NA significantly reduces inflammation in rat models of non-alcoholic steatohepatitis by lowering levels of tumor necrosis factor alpha (TNF- α) and NF- κ B.⁸³ As a precursor substance, NA effectively corrects NAD⁺ levels in tissues and improves mitochondrial metabolism as well as cachexia.⁸⁴ Numerous clinical studies have demonstrated that NA supplementation can increase NAD⁺ levels in host blood, enhance muscle strength and lean body mass, improve glucose homeostasis, and elevate mitochondrial biogenesis capacity.^{85–87} Host-derived nicotinamide can support microbial NAD biosynthesis, which is converted back to NA by microbes, absorbed by host intestinal tissues, and used to regenerate NAD through the Preiss-Handler pathway.⁸⁰ NAD⁺ is a crucial cofactor for mitochondrial function, which declines with age and may lead to impaired physical function.⁸⁸

The decline in cellular NAD levels is associated with mitochondrial and metabolic dysfunction.⁸⁹ These observations are consistent with our findings that the intake of *B. adolescentis* and NA significantly increases NAD⁺ levels in the serum and muscles of aged mice. Studies have shown that increasing NAD⁺ levels can enhance SIRT1 activity, inhibiting aging and related diseases.⁹⁰ Additionally, NAD⁺ attenuates mitochondrial damage through the SIRT1/PGC-1 α pathway and reduces ROS production in BV2 microglia.⁹¹ As observed in our study, the activation of SIRT1 promotes the expression of PGC-1 α , which increases mitochondrial quantity and function.⁹² This process enhances mitochondrial bioenergetics and boosts ATP production, thereby providing more energy to the cells.⁹³ Enhanced mitochondrial quantity and function increase energy production and improve muscle endurance and strength.^{94,95} These biological effects ultimately result in enhanced skeletal muscle function.

Figure 6. Nicotinic acid increases mitochondrial quantity and activity by generating NAD⁺ and activating the SIRT1/PGC-1 α axis

- (A) NAD⁺ content in the serum, TA, and soleus muscles of mice after nicotinic acid supplementation ($n = 6$ mice per group, Wilcoxon test).
- (B) Changes in SIRT1 gene expression in the TA and soleus muscles among different groups ($n = 6$ mice per group, Wilcoxon test).
- (C) Changes in PGC-1 α gene expression in the TA and soleus muscles among different groups ($n = 6$ mice per group, Wilcoxon test). Shown on the right are immunoblot analyses of protein lysates in the TA muscle of various groups of mice, indicating expression of PGC-1 α .
- (D) Changes in NRF1 and NRF2 gene expression in the TA muscle among different groups ($n = 6$ mice per group, Wilcoxon test).
- (E) Changes in mtDNA gene expression in the TA and soleus muscles among different groups ($n = 6$ mice per group, Wilcoxon test).
- (F) Changes in Tfam gene expression in the TA and soleus muscles among different groups ($n = 6$ mice per group, Wilcoxon test).
- (G) Comparison of citrate synthase activity in the TA and soleus muscles among different groups ($n = 6$ mice per group, Wilcoxon test).
- (H) Representative images of COX IV immunostaining in the TA muscle (green). The bar graph on the right shows the integrated fluorescence signal of COX IV immunofluorescence for each group. Immunostaining: scale bar, 150 μ m; magnification, $\times 25$. t test.
- Data are represented as mean \pm SEM. * $p < 0.05$, ** $p < 0.01$, and *** $p < 0.001$.



(legend on next page)

In conclusion, we demonstrate that NA produced by *B. adolescentis* promotes the proliferation of skeletal MUSCs and protects against muscle atrophy by increasing NAD⁺ levels and inhibiting the FoXO3/Atrogin-1/Murf-1 pathway. Alternatively, it activates the SIRT1/PGC-1 α pathway and enhances mitochondrial quantity and activity, thereby promoting oxidative metabolism in slow muscle fibers and improving overall skeletal muscle function. This finding provides a crucial basis for developing future probiotic-based strategies for treating sarcopenia. It underscores the significant role of the gut microbiome in the health of older adults.

Limitations of the study

Although this study provides insights into the role of *B. adolescentis* and NA in improving skeletal muscle function and mitochondrial activity, several limitations should be acknowledged. First, potential confounding factors, such as diet, may influence the observed effects. Second, this study only used male mice, which limits the generalizability of the findings to female mice. Future experiments are necessary to explore the potential sex-specific effects of *B. adolescentis* or NA in female mice. Third, the dexamethasone-induced muscle atrophy model is widely used and may also contribute to the decline in muscle mass during aging. We hypothesize that the dexamethasone model overlaps with sarcopenia in certain molecular mechanisms, particularly through the FoXO3 pathway and associated muscle protein degradation pathways. However, sarcopenia is a chronic, age-related condition, whereas dexamethasone-induced muscle atrophy involves acute glucocorticoid-driven pathways. Therefore, we acknowledge that this model has limitations in reflecting the complexity of gradual muscle loss during the aging process. Fourth, while we observed an increase in skeletal muscle mass following treatment, the exact mechanism linking mitochondrial function and muscle hypertrophy remains unclear. Although enhanced mitochondrial biogenesis and reduced atrophy-related signaling pathways (FoXO3/Atrogin-1/Murf-1) are involved, the roles of other processes are still uncertain. These gaps highlight the need for further mechanistic studies to provide a more comprehensive understanding in the future. Fifth, for the experiments involving human participants, although the focus of this study was not on sex or gender

differences, the lack of reporting on the influence (or association) of sex, gender, or both on the study outcomes is a limitation that may affect the generalizability of our findings to broader populations.

RESOURCE AVAILABILITY

Lead contact

Further information and requests for resources and data should be directed to and will be fulfilled by the lead contact, Jiachao Zhang (jiachao@hainanu.edu.cn).

Materials availability

This study did not generate new unique reagents.

Data and code availability

- The raw data for metabolomics quantitative analysis have been deposited in the MetaboLights and are publicly available as of the date of publication. Metagenomic data are publicly available in NCBI Sequence Read Archive under BioProject: PRJNA1140743. Accession numbers for NCBI and MetaboLights are listed in the [key resources table](#).
- This paper does not report original code.
- Uncropped western blots and original data for creating all graphs in the paper are provided in [Data S1](#). All datasets generated in this study can be obtained from the lead contact.

ACKNOWLEDGMENTS

This research was supported by the National Natural Science Foundation of China (32222066 and 32160545) and the Research Fund for the National Key R&D Program of China (2022YFD2100702). We would like to thank Shi Huang from the University of Hong Kong for his technical support and Min Zeng from Hainan General Hospital for her assistance with participant recruitment.

AUTHOR CONTRIBUTIONS

Conceptualization, J.Z., Z.Z., and Q.G.; methodology, J.Z., Z.Z., Z.Y., and Y.H.; investigation, Z.Z., Z.Y., S.J., Y.S., and J.L.; writing – original draft, Z.Z. and Z.Y.; writing – review & editing, J.Z., Z.Z., and Q.G.; funding acquisition, J.Z.; resources, J.Z.; supervision, J.Z.

DECLARATION OF INTERESTS

The authors report that there are no competing interests to declare.

Figure 7. Nicotinic acid supplementation enhances skeletal muscle oxidative metabolism

- (A) Comparison of mitochondrial respiratory chain complex I and II activity in the TA and soleus muscles among different groups ($n = 6$ mice per group, Wilcoxon test).
- (B) Comparison of ATP content in the TA and soleus muscles among different groups ($n = 6$ mice per group, Wilcoxon test).
- (C) ATP content in the serum of sarcopenia and healthy individuals based on untargeted metabolomics (*t* test).
- (D) The OCR levels of C2C12 cells in three groups. Wilcoxon test.
- (E) Representative immunostaining images of MyHC-I (green) and Laminin (red) in soleus muscle. Immunostaining: scale bar, 300 μ m; magnification, $\times 20$. Right: quantification of MyHC-I-positive fibers, presented as the percentage of MyHC-I-positive myofibers. *t* test.
- (F) Representative immunostaining images of MyHC-IIb (green) and Laminin (red) in TA muscle. Immunostaining: scale bar, 150 μ m; magnification, $\times 12$. Right: quantification of MyHC-IIb-positive fibers, presented as the percentage of MyHC-IIb-positive myofibers. *t* test.
- (G) Measurement of the CSA of MyHC-I-positive myofibers in soleus muscle. The values are presented as percentiles. *t* test. * indicates a significant difference compared to the young group: * $p < 0.05$, ** $p < 0.01$, and *** $p < 0.001$. # indicates a significant difference compared to the aged group: # $p < 0.05$, ### $p < 0.01$, and #### $p < 0.001$.
- (H) Measurement of the CSA of MyHC-IIb-positive myofibers in TA muscle. The values are presented as percentiles. *t* test. * indicates a significant difference compared to the young group: * $p < 0.05$, ** $p < 0.01$, and *** $p < 0.001$. # indicates a significant difference compared to the aged group: # $p < 0.05$, ### $p < 0.01$, and #### $p < 0.001$.
- Data are represented as mean \pm SEM.

STAR METHODS

Detailed methods are provided in the online version of this paper and include the following:

- **KEY RESOURCES TABLE**

- **EXPERIMENTAL MODEL AND STUDY PARTICIPANT DETAILS**

- Participant recruitment
- Bacterial culture
- Animal experiments
- Cell culture assay

- **METHOD DETAILS**

- Human biosample collection
- Fecal shotgun metagenomic sequencing
- Metagenomic species identification and functional annotation
- Selection of microbial species associated with sarcopenia
- Serum untargeted metabolomics analysis
- Nicotinic acid quantification
- Selection of microbial functions and metabolites associated with *B. adolescentis*
- Grip strength measurement in mice
- Treadmill task
- Histology
- Quantitative determination of nicotinic acid
- NAD⁺ measurement
- ATP content measurement
- Gene expression analysis by real-time quantitative RT-PCR
- Mitochondrial DNA copy number quantification
- Citrate synthase activity measurement
- Measurement of mitochondrial complex I and complex II
- Measurement of cellular OCR
- EdU assay for detection of proliferation in MUSCs
- Western blot analysis

- **QUANTIFICATION AND STATISTICAL ANALYSIS**

- **ADDITIONAL RESOURCES**

SUPPLEMENTAL INFORMATION

Supplemental information can be found online at <https://doi.org/10.1016/j.celrep.2025.115265>.

Received: August 16, 2024

Revised: November 29, 2024

Accepted: January 13, 2025

Published: February 4, 2025

REFERENCES

1. Chen, Y., and Wu, J. (2024). Aging-Related Sarcopenia: Metabolic Characteristics and Therapeutic Strategies. *Aging Dis.* <https://doi.org/10.14336/AD.2024.0407>.
2. Sun, J., Huang, J., and Lu, W. (2023). TT3, a more practical indicator for evaluating the relationship between sarcopenia and thyroid hormone in the euthyroid elderly compared with FT3. *Clin. Interv. Aging* **18**, 1361–1362. <https://doi.org/10.2147/CIA.S420558>.
3. Moon, S., Oh, C., Yu, J., Chung, H., Kim, Y., Lee, J., Kim, D., and Yu, J. (2023). IDF2022-0428 Effect of Sarcopenia on the risk of mortality according to metabolically healthy status and central obesity. *Diabetes Res. Clin. Pract.* **197**, 110418. <https://doi.org/10.1016/j.diabres.2023.110418>.
4. Atkins, J.L., and Wannamethee, S.G. (2020). Sarcopenic obesity in ageing: cardiovascular outcomes and mortality. *Br. J. Nutr.* **124**, 1102–1113. <https://doi.org/10.1017/S0007114520002172>.
5. Wu, J., Wang, K., Wang, X., Pang, Y., and Jiang, C. (2021). The role of the gut microbiome and its metabolites in metabolic diseases. *Protein Cell* **12**, 360–373. <https://doi.org/10.1007/s13238-020-00814-7>.
6. Wallrapp, A., and Chiu, I.M. (2024). Neuroimmune Interactions in the Intestine. *Annu. Rev. Immunol.* **42**, 489–519. <https://doi.org/10.1146/annurev-immunol-101921-042929>.
7. Frileux, S., Boltri, M., Doré, J., Leboyer, M., and Roux, P. (2024). Cognition and Gut microbiota in schizophrenia spectrum and mood disorders: A Systematic Review. *Neurosci. Biobehav. Rev.* **162**, 105722. <https://doi.org/10.1016/j.neubiorev.2024.105722>.
8. Fu, J., Qiu, W., Zheng, H., Qi, C., Hu, S., Wu, W., Wang, H., Wu, G., Cao, P., Ma, Z., et al. (2023). Ageing trajectory of the gut microbiota is associated with metabolic diseases in a chronological age-dependent manner. *Gut* **72**, 1431–1433. <https://doi.org/10.1136/gutnl-2022-328034>.
9. Cescon, M., Gambarotta, G., Calabro, S., Cicconetti, C., Anselmi, F., Kankowski, S., Lang, L., Basic, M., Bleich, A., Bolsega, S., et al. (2024). Gut microbiota depletion delays somatic peripheral nerve development and impairs neuromuscular junction maturation. *Gut Microb.* **16**, 2363015. <https://doi.org/10.1080/19490976.2024.2363015>.
10. Lustgarten, M.S. (2019). The role of the gut microbiome on skeletal muscle mass and physical function: 2019 update. *Front. Physiol.* **10**, 1435. <https://doi.org/10.3389/fphys.2019.01435>.
11. Winter, S.E., and Bäumler, A.J. (2023). Gut dysbiosis: Ecological causes and causative effects on human disease. *Proc. Natl. Acad. Sci. USA* **120**, e2316579120. <https://doi.org/10.1073/pnas.2316579120>.
12. Nikkhah, A., Ejtahed, H.-S., Ettehad Marvasti, F., Taghavi, M., Pakmehr, A., Hajipour, F., and Larjani, B. (2023). The critical role of gut microbiota dysbiosis in skeletal muscle wasting: a systematic review. *J. Appl. Microbiol.* **134**, lxac014. <https://doi.org/10.1093/jambo/lxac014>.
13. Chen, S., Huang, L., Liu, B., Duan, H., Li, Z., Liu, Y., Li, H., Fu, X., Lin, J., Xu, Y., et al. (2024). Dynamic changes in butyrate levels regulate satellite cell homeostasis by preventing spontaneous activation during aging. *Sci. China Life Sci.* **67**, 745–764. <https://doi.org/10.1007/s11427-023-2400-3>.
14. Saai, M., Li, A., McGlory, C., Stokes, T., von Allmen, M.T., Phillips, S.M., and Britz-McKibbin, P. (2019). Metabolic perturbations from step reduction in older persons at risk for sarcopenia: plasma biomarkers of abrupt changes in physical activity. *Metabolites* **9**, 134. <https://doi.org/10.3390/metabo9070134>.
15. Chen, L.H., Chang, S.S., Chang, H.Y., Wu, C.H., Pan, C.H., Chang, C.C., Chan, C.H., and Huang, H.Y. (2022). Probiotic supplementation attenuates age-related sarcopenia via the gut-muscle axis in SAMP8 mice. *J. Cachexia Sarcopenia Muscle* **13**, 515–531. <https://doi.org/10.1002/jcsm.12849>.
16. Liu, X., Wu, J., Tang, J., Xu, Z., Zhou, B., Liu, Y., Hu, F., Zhang, G., Cheng, R., Xia, X., et al. (2023). Prevotella copri alleviates sarcopenia via attenuating muscle mass loss and function decline. *J. Cachexia Sarcopenia Muscle* **14**, 2275–2288. <https://doi.org/10.1002/jcsm.13313>.
17. Zhang, C., Yu, L., Ma, C., Jiang, S., Zhang, Y., Wang, S., Tian, F., Xue, Y., Zhao, J., Zhang, H., et al. (2023). A key genetic factor governing arabinan utilization in the gut microbiome alleviates constipation. *Cell Host Microbe* **31**, 1989–2006.e8. <https://doi.org/10.1016/j.chom.2023.10.011>.
18. Zhao, L., Zhang, F., Ding, X., Wu, G., Lam, Y.Y., Wang, X., Fu, H., Xue, X., Lu, C., Ma, J., et al. (2018). Gut bacteria selectively promoted by dietary fibers alleviate type 2 diabetes. *Science* **359**, 1151–1156. <https://doi.org/10.1126/science.aao5774>.
19. Nagara, Y., Fujii, D., Takada, T., Sato-Yamazaki, M., Odani, T., and Oishi, K. (2022). Selective induction of human gut-associated acetogenic/butyrogenic microbiota based on specific microbial colonization of indigestible starch granules. *ISME J.* **16**, 1502–1511. <https://doi.org/10.1038/s41396-022-01196-w>.
20. Zhao, J., Huang, Y., and Yu, X. (2021). A narrative review of gut-muscle axis and sarcopenia: The potential role of gut microbiota. *Int. J. Gen. Med.* **14**, 1263–1273. <https://doi.org/10.2147/IJGM.S301141>.
21. Zhou, J., Liu, J., Lin, Q., Shi, L., Zeng, Z., Guan, L., Ma, Y., Zeng, Y., Zhong, S., and Xu, L. (2023). Characteristics of the gut microbiome and

- metabolic profile in elderly patients with sarcopenia. *Front. Pharmacol.* 14, 1279448. <https://doi.org/10.3389/fphar.2023.1279448>.
22. Liu, P., Jiang, Y., Gu, S., Xue, Y., Yang, H., Li, Y., Wang, Y., Yan, C., Jia, P., Lin, X., and Qi, G. (2021). Metagenome-wide association study of gut microbiome revealed potential microbial marker set for diagnosis of pediatric myasthenia gravis. *BMC Med.* 19, 159. <https://doi.org/10.1186/s12916-021-02034-0>.
 23. Moris, G., Arboleya, S., Mancabelli, L., Milani, C., Ventura, M., de Los Reyes-Gavilán, C.G., and Gueimonde, M. (2018). Fecal microbiota profile in a group of myasthenia gravis patients. *Sci. Rep.* 8, 14384. <https://doi.org/10.1038/s41598-018-32700-y>.
 24. Ni, Y., Lohinai, Z., Heshiki, Y., Dorne, B., Moldvay, J., Dulka, E., Galffy, G., Berta, J., Weiss, G.J., Sommer, M.O.A., and Panagiotou, G. (2021). Distinct composition and metabolic functions of human gut microbiota are associated with cachexia in lung cancer patients. *ISME J.* 15, 3207–3220. <https://doi.org/10.1038/s41396-021-00998-8>.
 25. Chen, S., Chen, L., Qi, Y., Xu, J., Ge, Q., Fan, Y., Chen, D., Zhang, Y., Wang, L., Hou, T., et al. (2021). *Bifidobacterium adolescentis* regulates catalase activity and host metabolism and improves healthspan and lifespan in multiple species. *Nat. Aging* 1, 991–1001. <https://doi.org/10.1038/s43587-021-00129-0>.
 26. Sugimura, Y., Kanda, A., Sawada, K., Wai, K.M., Tanabu, A., Ozato, N., Midorikawa, T., Hisada, T., Nakaji, S., and Ihara, K. (2022). Association between Gut Microbiota and Body Composition in Japanese General Population: A Focus on Gut Microbiota and Skeletal Muscle. *Int. J. Environ. Res. Publ. Health* 19, 7464. <https://doi.org/10.3390/ijerph19127464>.
 27. Wang, Z., Xu, X., Deji, Y., Gao, S., Wu, C., Song, Q., Shi, Z., Xiang, X., Zang, J., and Su, J. (2023). *Bifidobacterium* as a Potential Biomarker of Sarcopenia in Elderly Women. *Nutrients* 15, 1266. <https://doi.org/10.3390/nu15051266>.
 28. Shan, Z., Cheng, N., Zhu, J., Chen, F., and Ji, J.; Meilibaba (2024). Analysis of intestinal flora in elderly Uygur patients with sarcopenia. *Immun. Inflamm. Dis.* 12, e1097. <https://doi.org/10.1002/iid3.1097>.
 29. Rinaldi, E., Consonni, A., Cordigliero, C., Sacco, G., Crasà, C., Fontana, A., Morelli, L., Elli, M., Mantegazza, R., and Baggi, F. (2019). Therapeutic Effect of *Bifidobacterium* Administration on Experimental Autoimmune Myasthenia Gravis in Lewis Rats. *Front. Immunol.* 10, 2949. <https://doi.org/10.3389/fimmu.2019.02949>.
 30. Bae, S.S., Dong, T.S., Wang, J., Lagishetty, V., Katzka, W., Jacobs, J.P., and Charles-Schoeman, C. (2022). Altered gut microbiome in patients with dermatomyositis. *ACR Open Rheumatol.* 4, 658–670. <https://doi.org/10.1002/acr2.11436>.
 31. Bindels, L.B., Neyrinck, A.M., Claus, S.P., Le Roy, C.I., Grangette, C., Pot, B., Martinez, I., Walter, J., Cani, P.D., and Delzenne, N.M. (2016). Synbiotic approach restores intestinal homeostasis and prolongs survival in leukaemic mice with cachexia. *ISME J.* 10, 1456–1470. <https://doi.org/10.1038/ismej.2015.209>.
 32. Ni, Y., Yang, X., Zheng, L., Wang, Z., Wu, L., Jiang, J., Yang, T., Ma, L., and Fu, Z. (2019). *Lactobacillus* and *Bifidobacterium* improves physiological function and cognitive ability in aged mice by the regulation of gut microbiota. *Mol. Nutr. Food Res.* 63, 1900603. <https://doi.org/10.1002/mnfr.201900603>.
 33. Ye, H., Ghosh, T.S., Hueston, C.M., Vickova, K., Golubeva, A.V., Hyland, N.P., and O'Toole, P.W. (2023). Engraftment of aging-related human gut microbiota and the effect of a seven-species consortium in a pre-clinical model. *Gut Microb.* 15, 2282796. <https://doi.org/10.1080/19490976.2023.2282796>.
 34. Sakakida, T., Ishikawa, T., Doi, T., Morita, R., Endo, Y., Matsumura, S., Ota, T., Yoshida, J., Hirai, Y., Mizushima, K., et al. (2022). Water-soluble dietary fiber alleviates cancer-induced muscle wasting through changes in gut microenvironment in mice. *Cancer Sci.* 113, 1789–1800. <https://doi.org/10.1111/cas.15306>.
 35. Lou, J., Wang, Q., Wan, X., and Cheng, J. (2024). Changes and correlation analysis of intestinal microflora composition, inflammatory index, and skeletal muscle mass in elderly patients with sarcopenia. *Geriatr. Gerontol. Int.* 24, 140–146. <https://doi.org/10.1111/ggi.14661>.
 36. Zhang, H., Ryu, D., Wu, Y., Gariani, K., Wang, X., Luan, P., D'Amico, D., Ropelle, E.R., Lutolf, M.P., Aebersold, R., et al. (2016). NAD+ repletion improves mitochondrial and stem cell function and enhances life span in mice. *Science* 352, 1436–1443. <https://doi.org/10.1126/science.aaf2693>.
 37. Hughes, D.C., Marcotte, G.R., Marshall, A.G., West, D.W.D., Baehr, L.M., Wallace, M.A., Saleh, P.M., Bodine, S.C., and Baar, K. (2017). Age-related differences in dystrophin: impact on force transfer proteins, membrane integrity, and neuromuscular junction stability. *J. Gerontol. A Biol. Sci. Med. Sci.* 72, 640–648. <https://doi.org/10.1093/gerona/glw109>.
 38. Zhao, J., Brault, J.J., Schild, A., Cao, P., Sandri, M., Schiaffino, S., Lecker, S.H., and Goldberg, A.L. (2007). FoxO3 coordinately activates protein degradation by the autophagic/lysosomal and proteasomal pathways in atrophying muscle cells. *Cell Metabol.* 6, 472–483. <https://doi.org/10.1016/j.cmet.2007.11.004>.
 39. Li, G., Jin, B., and Fan, Z. (2022). Mechanisms involved in gut microbiota regulation of skeletal muscle. *Oxid. Med. Cell. Longev.* 2022, 2151191. <https://doi.org/10.1155/2022/2151191>.
 40. Tuchaai, E., Endres, V., Jones, B., Shankar, S., Klemashevich, C., Sun, Y., and Wu, C.-S. (2022). Deletion of ghrelin alters tryptophan metabolism and exacerbates experimental ulcerative colitis in aged mice. *Exp. Biol. Med.* 247, 1558–1569. <https://doi.org/10.1177/15353702221110647>.
 41. Sauve, A.A. (2008). NAD+ and vitamin B3: from metabolism to therapies. *J. Pharmacol. Exp. Therapeut.* 324, 883–893. <https://doi.org/10.1124/jpet.107.120758>.
 42. Graboski, A.L., Kowalewski, M.E., Simpson, J.B., Cao, X., Ha, M., Zhang, J., Walton, W.G., Flaherty, D.P., and Redinbo, M.R. (2023). Mechanism-based inhibition of gut microbial tryptophanases reduces serum indoxyl sulfate. *Cell Chem. Biol.* 30, 1402–1413.e7. <https://doi.org/10.1016/j.chembiol.2023.07.015>.
 43. Enoki, Y., Watanabe, H., Arake, R., Sugimoto, R., Imafuku, T., Tominaga, Y., Ishima, Y., Kotani, S., Nakajima, M., Tanaka, M., et al. (2016). Indoxyl sulfate potentiates skeletal muscle atrophy by inducing the oxidative stress-mediated expression of myostatin and atrogin-1. *Sci. Rep.* 6, 32084. <https://doi.org/10.1038/srep32084>.
 44. Liu, S., Sun, Y., Zhao, R., Wang, Y., Zhang, W., and Pang, W. (2021). Isoleucine increases muscle mass through promoting myogenesis and intramyocellular fat deposition. *Food Funct.* 12, 144–153. <https://doi.org/10.1039/d0fo02156c>.
 45. Hofer, S.J., Daskalaki, I., Bergmann, M., Friščić, J., Zimmermann, A., Müller, M.I., Abdellatif, M., Nicastro, R., Masser, S., Durand, S., et al. (2024). Spermidine is essential for fasting-mediated autophagy and longevity. *Nat. Cell Biol.* 26, 1571–1584. <https://doi.org/10.1038/s41556-024-01468-x>.
 46. Hernandez-Benitez, R., Wang, C., Shi, L., Ouchi, Y., Zhong, C., Hishida, T., Liao, H.-K., Magill, E.A., Memczak, S., Soligalla, R.D., et al. (2024). Intervention with metabolites emulating endogenous cell transitions accelerates muscle regeneration in young and aged mice. *Cell Rep. Med.* 5, 101449. <https://doi.org/10.1016/j.xcrm.2024.101449>.
 47. Książek, A., Zagrodna, A., and Stowińska-Lisowska, M. (2019). Vitamin D, skeletal muscle function and athletic performance in athletes—A narrative review. *Nutrients* 11, 1800. <https://doi.org/10.3390/nu11081800>.
 48. Jin, H., Oh, H.-J., and Lee, B.-Y. (2023). GABA prevents age-related sarcopenic obesity in mice with high-fat-diet-induced obesity. *Cells* 12, 2146. <https://doi.org/10.3390/cells12172146>.
 49. Liu, J., Peng, Y., Wang, X., Fan, Y., Qin, C., Shi, L., Tang, Y., Cao, K., Li, H., Long, J., and Liu, J. (2016). Mitochondrial dysfunction launches dexamethasone-induced skeletal muscle atrophy via AMPK/FOXO3 signaling. *Mol. Pharm.* 13, 73–84. <https://doi.org/10.1021/acs.molpharmaceut.5b00516>.

50. Lahiri, S., Kim, H., Garcia-Perez, I., Reza, M.M., Martin, K.A., Kundu, P., Cox, L.M., Selkirk, J., Posma, J.M., Zhang, H., et al. (2019). The gut microbiota influences skeletal muscle mass and function in mice. *Sci. Transl. Med.* 11, eaan5662. <https://doi.org/10.1126/scitranslmed.aan5662>.
51. Shen, C., Cai, G.-Q., Peng, J.-P., and Chen, X.-D. (2015). Autophagy protects chondrocytes from glucocorticoids-induced apoptosis via ROS/Akt/FOXO3 signaling. *Osteoarthritis Cartilage* 23, 2279–2287. <https://doi.org/10.1016/j.joca.2015.06.020>.
52. Wuerch, E., Urquiza, G.R., and Yong, V.W. (2023). The promise of niacin in neurology. *Neurotherapeutics* 20, 1037–1054. <https://doi.org/10.1007/s13311-023-01376-2>.
53. Anderson, R.M., Barger, J.L., Edwards, M.G., Braun, K.H., O'Connor, C.E., Prolla, T.A., and Weindruch, R. (2008). Dynamic regulation of PGC-1 α localization and turnover implicates mitochondrial adaptation in calorie restriction and the stress response. *Aging Cell* 7, 101–111. <https://doi.org/10.1111/j.1474-9726.2007.00357.x>.
54. Andres, A.M., Stotland, A., Quelliconi, B.B., and Gottlieb, R.A. (2015). A time to reap, a time to sow: mitophagy and biogenesis in cardiac pathophysiology. *J. Mol. Cell. Cardiol.* 78, 62–72. <https://doi.org/10.1016/j.yjmcc.2014.10.003>.
55. Shi, Y., Dierckx, A., Wanrooij, P.H., Wanrooij, S., Larsson, N.-G., Wilhelmsson, L.M., Falkenberg, M., and Gustafsson, C.M. (2012). Mammalian transcription factor A is a core component of the mitochondrial transcription machinery. *Proc. Natl. Acad. Sci. USA* 109, 16510–16515. <https://doi.org/10.1073/pnas.1119738109>.
56. Bae, J.-H., Jo, A., Cho, S.C., Lee, Y.-I., Kam, T.-I., You, C.-L., Jeong, H.-J., Kim, H., Jeong, M.-H., Jeong, Y., et al. (2023). Farnesol prevents aging-related muscle weakness in mice through enhanced farnesylation of Parkin-interacting substrate. *Sci. Transl. Med.* 15, eab3489. <https://doi.org/10.1126/scitranslmed.abh3489>.
57. Kang, C., and Ji, L.L. (2013). Role of PGC-1 α in muscle function and aging. *Journal of Sport and Health Science* 2, 81–86. <https://doi.org/10.1016/j.jshs.2013.03.005>.
58. Arany, Z. (2008). PGC-1 coactivators and skeletal muscle adaptations in health and disease. *Curr. Opin. Genet. Dev.* 18, 426–434. <https://doi.org/10.1016/j.gde.2008.07.018>.
59. Geng, T., Li, P., Yin, X., and Yan, Z. (2011). PGC-1 α promotes nitric oxide antioxidant defenses and inhibits FOXO signaling against cardiac cachexia in mice. *Am. J. Pathol.* 178, 1738–1748. <https://doi.org/10.1016/ajpath.2011.01.005>.
60. Sandri, M., Lin, J., Handschin, C., Yang, W., Arany, Z.P., Lecker, S.H., Goldberg, A.L., and Spiegelman, B.M. (2006). PGC-1 α protects skeletal muscle from atrophy by suppressing FoxO3 action and atrophy-specific gene transcription. *Proc. Natl. Acad. Sci. USA* 103, 16260–16265. <https://doi.org/10.1073/pnas.0607795103>.
61. Alexander, M.S., Rozkalne, A., Colletta, A., Spinazzola, J.M., Johnson, S., Rahimov, F., Meng, H., Lawlor, M.W., Estrella, E., Kunkel, L.M., and Gussoni, E. (2016). CD82 is a marker for prospective isolation of human muscle satellite cells and is linked to muscular dystrophies. *Cell Stem Cell* 19, 800–807. <https://doi.org/10.1016/j.stem.2016.08.006>.
62. Alway, S.E., Myers, M.J., and Mohamed, J.S. (2014). Regulation of satellite cell function in sarcopenia. *Front. Aging Neurosci.* 6, 246. <https://doi.org/10.3389/fnagi.2014.00246>.
63. Liu, L., Hu, R., You, H., Li, J., Liu, Y., Li, Q., Wu, X., Huang, J., Cai, X., Wang, M., and Wei, L. (2021). Formononetin ameliorates muscle atrophy by regulating myostatin-mediated PI3K/Akt/FoxO3a pathway and satellite cell function in chronic kidney disease. *J. Cell Mol. Med.* 25, 1493–1506. <https://doi.org/10.1111/jcmm.16238>.
64. Gan, W., He, H., and Li, L. (2016). Molecular cloning, characterisation and functional analysis of the duck Forkhead box O3 (FOXO3) gene. *Br. Poultry Sci.* 57, 143–150. <https://doi.org/10.1080/00071668.2015.1135503>.
65. Hagenbuchner, J., Kuznetsov, A., Hermann, M., Hausott, B., Obexer, P., and Ausserlechner, M.J. (2012). FOXO3-induced reactive oxygen species are regulated by BCL2L11 (Bim) and SESN3. *J. Cell Sci.* 125, 1191–1203. <https://doi.org/10.1242/jcs.092098>.
66. Hagenbuchner, J., and Ausserlechner, M.J. (2013). Mitochondria and FOXO3: breath or die. *Front. Physiol.* 4, 147. <https://doi.org/10.3389/fphys.2013.00147>.
67. Shan, X.-q., Zhou, N., Pei, C.-x., Lu, X., Chen, C.-p., and Chen, H.-q. (2024). Tetrandrine induces muscle atrophy involving ROS-mediated inhibition of Akt and FoxO3. *Mol. Med.* 30, 218. <https://doi.org/10.1186/s10020-024-00981-x>.
68. Scicchitano, B.M., Pelosi, L., Sica, G., and Musarò, A. (2018). The physiopathologic role of oxidative stress in skeletal muscle. *Mech. Ageing Dev.* 170, 37–44. <https://doi.org/10.1016/j.mad.2017.08.009>.
69. Narasimhan, M., Hong, J., Atieno, N., Muthusamy, V.R., Davidson, C.J., Abu-Rmaileh, N., Richardson, R.S., Gomes, A.V., Hoidal, J.R., and Rajasekaran, N.S. (2014). Nrf2 deficiency promotes apoptosis and impairs PAX7/MyoD expression in aging skeletal muscle cells. *Free Radic. Biol. Med.* 71, 402–414. <https://doi.org/10.1016/j.freeradbiomed.2014.02.023>.
70. Ticinesi, A., Lauretani, F., Milani, C., Nouvenne, A., Tana, C., Del Rio, D., Maggio, M., Ventura, M., and Meschi, T. (2017). Aging gut microbiota at the cross-road between nutrition, physical frailty, and sarcopenia: is there a gut-muscle axis? *Nutrients* 9, 1303. <https://doi.org/10.3390/nu9121303>.
71. Grosicki, G.J., Fielding, R.A., and Lustgarten, M.S. (2018). Gut microbiota contribute to age-related changes in skeletal muscle size, composition, and function: biological basis for a gut-muscle axis. *Calcif. Tissue Int.* 102, 433–442. <https://doi.org/10.1007/s00223-017-0345-5>.
72. Xiao, Y., Yang, C., Yu, L., Tian, F., Wu, Y., Zhao, J., Zhang, H., Yang, R., Chen, W., Hill, C., et al. (2021). Human gut-derived *B. longum* subsp. *longum* strains protect against aging in ad-galactose-induced aging mouse model. *Microbiome* 9, 180. <https://doi.org/10.1186/s40168-021-01108-8>.
73. Drago, L., Toscano, M., Rodighiero, V., De Vecchi, E., and Mogna, G. (2012). Cultivable and pyrosequenced fecal microflora in centenarians and young subjects. *J. Clin. Gastroenterol.* 46, S81–S84. <https://doi.org/10.1097/MCG.0b013e3182693982>.
74. Zeng, Y., He, X., Peng, X., Zhao, L., Yin, C., and Mao, S. (2024). Combined Nutrition with Exercise: Fueling the Fight Against Sarcopenia Through a Bibliometric Analysis and Review. *Int. J. Gen. Med.* 17, 1861–1876. <https://doi.org/10.2147/IJGM.S462594>.
75. Wang, L., Hu, L., Xu, Q., Yin, B., Fang, D., Wang, G., Zhao, J., Zhang, H., and Chen, W. (2017). *Bifidobacterium adolescentis* exerts strain-specific effects on constipation induced by loperamide in BALB/c mice. *Int. J. Mol. Sci.* 18, 318. <https://doi.org/10.3390/ijms18020318>.
76. Fan, L., Qi, Y., Qu, S., Chen, X., Li, A., Hendi, M., Xu, C., Wang, L., Hou, T., Si, J., and Chen, S. (2021). *B. adolescentis* ameliorates chronic colitis by regulating Treg/Th2 response and gut microbiota remodeling. *Gut Microb.* 13, 1–17. <https://doi.org/10.1080/19490976.2020.1826746>.
77. Ticinesi, A., Nouvenne, A., Cerundolo, N., Catania, P., Prati, B., Tana, C., and Meschi, T. (2019). Gut microbiota, muscle mass and function in aging: a focus on physical frailty and sarcopenia. *Nutrients* 11, 1633. <https://doi.org/10.3390/nu11071633>.
78. Shats, I., Williams, J.G., Liu, J., Makarov, M.V., Wu, X., Lih, F.B., Deterding, L.J., Lim, C., Xu, X., Randall, T.A., et al. (2020). Bacteria boost mammalian host NAD metabolism by engaging the deamidated biosynthesis pathway. *Cell Metabol.* 31, 564–579.e7. <https://doi.org/10.1016/j.cmet.2020.02.001>.
79. Lin, H., Kwan, A.L., and Dutcher, S.K. (2010). Synthesizing and salvaging NAD $^+$: lessons learned from *Chlamydomonas reinhardtii*. *PLoS Genet.* 6, e1001105. <https://doi.org/10.1371/journal.pgen.1001105>.

80. Chellappa, K., McReynolds, M.R., Lu, W., Zeng, X., Makarov, M., Hayat, F., Mukherjee, S., Bhat, Y.R., Lingala, S.R., Shima, R.T., et al. (2022). NAD precursors cycle between host tissues and the gut microbiome. *Cell Metabol.* 34, 1947–1959.e5. <https://doi.org/10.1016/j.cmet.2022.11.004>.
81. Wang, Y., Wu, J., Lv, M., Shao, Z., Hungwe, M., Wang, J., Bai, X., Xie, J., Wang, Y., and Geng, W. (2021). Metabolism characteristics of lactic acid bacteria and the expanding applications in food industry. *Front. Bioeng. Biotechnol.* 9, 612285. <https://doi.org/10.3389/fbioe.2021.612285>.
82. Ringseis, R., Gessner, D.K., Beer, A.M., Albrecht, Y., Wen, G., Most, E., Krüger, K., and Eder, K. (2020). Nicotinic acid improves endurance performance of mice subjected to treadmill exercise. *Metabolites* 10, 138. <https://doi.org/10.3390/metabo10040138>.
83. Lukasova, M., Malaval, C., Gille, A., Kero, J., and Offermanns, S. (2011). Nicotinic acid inhibits progression of atherosclerosis in mice through its receptor GPR109A expressed by immune cells. *J. Clin. Invest.* 121, 1163–1173. <https://doi.org/10.1172/JCI41651>.
84. Beltrà, M., Pöllänen, N., Fornelli, C., Tonttila, K., Hsu, M.Y., Zampieri, S., Moletta, L., Corrà, S., Porporato, P.E., Kivelä, R., et al. (2023). NAD+ repletion with niacin counteracts cancer cachexia. *Nat. Commun.* 14, 1849. <https://doi.org/10.1038/s41467-023-37595-6>.
85. Pirinen, E., Auranen, M., Khan, N.A., Brilhante, V., Urho, N., Pessia, A., Hakkarainen, A., Kuula, J., Heinonen, U., Schmidt, M.S., et al. (2020). Niacin cures systemic NAD+ deficiency and improves muscle performance in adult-onset mitochondrial myopathy. *Cell Metabol.* 31, 1078–1090.e5. <https://doi.org/10.1016/j.cmet.2020.04.008>.
86. Xiang, S., Li, Y., Li, Y., Zhang, J., Pan, W., Lu, Y., and Liu, S. (2023). Increased dietary niacin intake improves muscle strength, quality, and glucose homeostasis in adults over 40 years of age. *J. Nutr. Health Aging* 27, 709–718. <https://doi.org/10.1007/s12603-023-1967-0>.
87. Borda, M.G., Samuelsson, J., Cederholm, T., Baldera, J.P., Pérez-Zepeda, M.U., Barreto, G.E., Zettergren, A., Kern, S., Rydén, L., González-Lara, M., et al. (2024). Nutrient Intake and Its Association with Appendicular Total Lean Mass and Muscle Function and Strength in Older Adults: A Population-Based Study. *Nutrients* 16, 568. <https://doi.org/10.3390/nu16040568>.
88. Seldeen, K.L., Shahini, A., Thiagarajan, R., Redae, Y., Leiker, M., Rajabian, N., Dynka, A., Andreadis, S.T., and Troen, B.R. (2021). Short-term nicotinamide riboside treatment improves muscle quality and function in mice and increases cellular energetics and differentiating capacity of myogenic progenitors. *Nutrition* 87–88, 111189. <https://doi.org/10.1016/j.nut.2021.111189>.
89. Srivastava, S. (2016). Emerging therapeutic roles for NAD+ metabolism in mitochondrial and age-related disorders. *Clin. Transl. Med.* 5, 25. <https://doi.org/10.1186/s40169-016-0104-7>.
90. Gong, H., Chen, H., Xiao, P., Huang, N., Han, X., Zhang, J., Yang, Y., Li, T., Zhao, T., Tai, H., et al. (2022). miR-146a impedes the anti-aging effect of AMPK via NAMPT suppression and NAD+/SIRT inactivation. *Signal Transduct. Targeted Ther.* 7, 66. <https://doi.org/10.1038/s41392-022-00886-3>.
91. Zhao, Y., Zhang, J., Zheng, Y., Zhang, Y., Zhang, X.J., Wang, H., Du, Y., Guan, J., Wang, X., and Fu, J. (2021). NAD+ improves cognitive function and reduces neuroinflammation by ameliorating mitochondrial damage and decreasing ROS production in chronic cerebral hypoperfusion models through Sirt1/PGC-1 α pathway. *J. Neuroinflammation* 18, 207. <https://doi.org/10.1186/s12974-021-02250-8>.
92. Fan, W., and Evans, R. (2015). PPARs and ERRs: molecular mediators of mitochondrial metabolism. *Curr. Opin. Cell Biol.* 33, 49–54. <https://doi.org/10.1016/j.cub.2014.11.002>.
93. Wallace, D.C. (2018). Mitochondrial genetic medicine. *Nat. Genet.* 50, 1642–1649. <https://doi.org/10.1038/s41588-018-0264-z>.
94. Chen, X., Luo, Y., Zhu, Q., Zhang, J., Huang, H., Kan, Y., Li, D., Xu, M., Liu, S., Li, J., et al. (2024). Small extracellular vesicles from young plasma reverse age-related functional declines by improving mitochondrial energy metabolism. *Nat. Aging* 4, 814–838. <https://doi.org/10.1038/s43587-024-00612-4>.
95. Sopariwala, D.H., Rios, A.S., Pei, G., Roy, A., Tomaz da Silva, M., Thi Thu Nguyen, H., Saley, A., Van Drunen, R., Kralli, A., Mahan, K., et al. (2023). Innately expressed estrogen-related receptors in the skeletal muscle are indispensable for exercise fitness. *Faseb. J.* 37, e22727. <https://doi.org/10.1096/fj.202201518R>.
96. Shannon, P., Markiel, A., Ozier, O., Baliga, N.S., Wang, J.T., Ramage, D., Amin, N., Schwikowski, B., and Ideker, T. (2003). Cytoscape: a software environment for integrated models of biomolecular interaction networks. *Genome Res.* 13, 2498–2504. <https://doi.org/10.1101/gr.123930>.
97. Beghini, F., McIver, L.J., Blanco-Míguez, A., Dubois, L., Asnicar, F., Maharanj, S., Mailyan, A., Manghi, P., Scholz, M., Thomas, A.M., et al. (2021). Integrating taxonomic, functional, and strain-level profiling of diverse microbial communities with bioBakery 3. *Elife* 10, e65088. <https://doi.org/10.7554/eLife.65088>.
98. Jiang, S., Du, L., Zhao, Q., Su, S., Huang, S., and Zhang, J. (2024). Tropical postbiotics alleviate the disorders in the gut microbiota and kidney damage induced by ochratoxin A exposure. *Food Funct.* 15, 3980–3992. <https://doi.org/10.1039/d3fo05213c>.
99. Jin, H., Quan, K., He, Q., Kwok, L.Y., Ma, T., Li, Y., Zhao, F., You, L., Zhang, H., and Sun, Z. (2023). A high-quality genome compendium of the human gut microbiome of Inner Mongolians. *Nat. Microbiol.* 8, 150–161. <https://doi.org/10.1038/s41564-022-01270-1>.
100. Karp, P.D., Billington, R., Caspi, R., Fulcher, C.A., Latendresse, M., Kothoni, A., Keseler, I.M., Krummenacker, M., Midford, P.E., Ong, Q., et al. (2019). The BioCyc collection of microbial genomes and metabolic pathways. *Briefings Bioinf.* 20, 1085–1093. <https://doi.org/10.1093/bib/bbx085>.
101. Jiang, S., Chen, D., Ma, C., Liu, H., Huang, S., and Zhang, J. (2022). Establishing a novel inflammatory bowel disease prediction model based on gene markers identified from single nucleotide variants of the intestinal microbiota. *iMeta* 1, e40. <https://doi.org/10.1002/imt2.40>.
102. Giebultowicz, J., Korytowska, N., Sankowski, B., and Wroczyński, P. (2016). Development and validation of a LC-MS/MS method for quantitative analysis of uraemic toxins p-cresol sulphate and indoxyl sulphate in saliva. *Talanta* 150, 593–598. <https://doi.org/10.1016/j.talanta.2015.12.075>.
103. Liang, L., Rasmussen, M.-L.H., Piening, B., Shen, X., Chen, S., Röst, H., Snyder, J.K., Tibshirani, R., Skotte, L., Lee, N.C., et al. (2020). Metabolic dynamics and prediction of gestational age and time to delivery in pregnant women. *Cell* 181, 1680–1692.e15. <https://doi.org/10.1016/j.cell.2020.05.002>.
104. Yu, G., Xu, C., Zhang, D., Ju, F., and Ni, Y. (2022). MetOrigin: discriminating the origins of microbial metabolites for integrative analysis of the gut microbiome and metabolome. *iMeta* 1, e10. <https://doi.org/10.1002/imt2.10>.
105. Zhang, Z., Li, J., Jiang, S., Xu, M., Ma, T., Sun, Z., and Zhang, J. (2023). Lactobacillus fermentum HNU312 alleviated oxidative damage and behavioural abnormalities during brain development in early life induced by chronic lead exposure. *Ecotox Environ Safe* 251, 114543. <https://doi.org/10.1016/j.ecoenv.2023.114543>.
106. Shang, G.K., Han, L., Wang, Z.H., Liu, Y.P., Yan, S.B., Sai, W.W., Wang, D., Li, Y.H., Zhang, W., and Zhong, M. (2020). Sarcopenia is attenuated by TRB3 knockout in aging mice via the alleviation of atrophy and fibrosis of skeletal muscles. *J. Cachexia Sarcopenia Muscle* 11, 1104–1120. <https://doi.org/10.1002/jscm.12560>.
107. Sanz-Ros, J., Romero-García, N., Mas-Bargues, C., Monleón, D., Gordejicus, J., Brooke, R.T., Dromant, M., Díaz, A., Derevyanko, A., Guió-Carrión, A., et al. (2022). Small extracellular vesicles from young adipose-derived stem cells prevent frailty, improve health span, and decrease

- epigenetic age in old mice. *Sci. Adv.* 8, eabq2226. <https://doi.org/10.1126/sciadv.abq2226>.
108. Decosterd, L.A., Mercier, T., Ternon, B., Cruchon, S., Guignard, N., Lahrichi, S., Pesse, B., Rochat, B., Burger, R., Lamoth, F., et al. (2020). Validation and clinical application of a multiplex high performance liquid chromatography-tandem mass spectrometry assay for the monitoring of plasma concentrations of 12 antibiotics in patients with severe bacte-
- rial infections. *J. Chromatogr. B* 1157, 122160. <https://doi.org/10.1016/j.jchromb.2020.122160>.
109. Saito, K., Sekiya, M., Kainoh, K., Yoshino, R., Hayashi, A., Han, S.-I., Araki, M., Ohno, H., Takeuchi, Y., Tsuyuzaki, T., et al. (2023). Obesity-induced metabolic imbalance allosterically modulates CtBP2 to inhibit PPAR-alpha transcriptional activity. *J. Biol. Chem.* 299, 104890. <https://doi.org/10.1016/j.jbc.2023.104890>.

STAR★METHODS

KEY RESOURCES TABLE

REAGENT or RESOURCE	SOURCE	IDENTIFIER
Antibodies		
Anti-coxIV	Servicebio	Cat#: GB15250; RRID: N/A
Alexa Fluor 488-labeled goat anti-mouse IgG	Servicebio	Cat#: GB25301; RRID: AB_2904018
Anti-Dystrophin	Servicebio	Cat#: GB112953; RRID: N/A
CY3-labeled goat anti-rabbit IgG	Servicebio	Cat#: GB21303; RRID: AB_2861435
HRP-labeled goat anti-rabbit IgG	Servicebio	Cat#: GB23204; RRID: AB_2938981
Anti-PAX7	Servicebio	Cat#: GB113190; RRID: N/A
Alexa Fluor 488-labeled goat anti-rabbit IgG	Servicebio	Cat#: GB25303 RRID: AB_2910224
Anti-GAPDH	Servicebio	Cat#: GB15004 RRID: AB_2943040
Anti-PGC-1 α	Servicebio	Cat#: GB11912; RRID: N/A
Anti-FoxO3	Servicebio	Cat#: GB11092; RRID: N/A
Anti-MYH4	Poteintech	Cat#: 20140-1-AP; RRID: AB_10666434
Anti-Laminin	Sigma-Aldrich	Cat#: L9393; RRID: AB_477163
Anti-MYH7	Servicebio	Cat#: GB121857; RRID: N/A
Bacterial and virus strains		
Bifidobacterium adolescentis ATCC15703	Guangdong Microbial Culture Collection Center	Cat#: ATCC15703
Biological samples		
Human fecal samples	This paper	N/A
Human blood samples	This paper	N/A
Mice fecal samples	This paper	N/A
Mice blood samples	This paper	N/A
Mice tissue samples	This paper	N/A
Chemicals, peptides, and recombinant proteins		
Nicotinic acid	Aladdin Biochemical Technology	Cat#: N103652-25
SYBR Qpcr Master mix	Vazyme Biotech Co., Ltd	Cat#: Q711
TRIZOL reagent	Thermo Fisher Scientific	Cat#: 15596026CN
TPY medium	HuanKai Biology	Cat#: 027350
DAPI	Servicebio	Cat#: G1012
Dewaxing solution	Servicebio	Cat#: G1128
Sodium citrate antigen repair solution	Servicebio	Cat#: G1202
EDTA Antigen Repair Solution (PH9.0)	Servicebio	Cat#: G1203
EDTA Antigen Repair Solution (PH8.0)	Servicebio	Cat#: G1206
Tissue autofluorescence quencher	Servicebio	Cat#: G1221
Bovine Serum Albumin BSA	Servicebio	Cat#: GC305010
Anti-fluorescence quenching encapsulant	Servicebio	Cat#: G1401
RIPA lysis solution	Servicebio	Cat#: G2002
Phosphorylated protease inhibitors	Servicebio	Cat#: G2007
5×Protein Sampling Buffer	Servicebio	Cat#: G2075
Prestained Protein Marker	Servicebio	Cat#: G2087
PVDF membrane	Servicebio	Cat#: G6015

(Continued on next page)

Continued

REAGENT or RESOURCE	SOURCE	IDENTIFIER
Critical commercial assays		
QIAamp® DNA Stool Mini Kit	Qiagen	Cat#: 51504
Revert Aid First Strand cDNA synthesis kit	Thermo Fisher Scientific	Cat#: K1622
NAD+ Assay Kit in Animal Tissue	Beyotime Biotechnology	Cat#: S0176S
NAD+ Assay Kit in Serum	Nanjing Jiancheng Bioengineering Institute	Cat#: A114-1-1
ATP content Assay Kit	Nanjing Jiancheng Bioengineering Institute	Cat#: A095-1-1
Citrate synthase activity Assay Kit	Nanjing Jiancheng Bioengineering Institute	Cat#: A108-1-2
Mitochondrial Complex I activity assay kit	Solarbio	Cat#: BC0510
Complex II activity assay kit	Solarbio	Cat#: BC3230
10% PAGE Gel Quick Preparation Kit	Servicebio	Cat#: G2043
BCA protein quantification kit	Servicebio	Cat#: G2026
BCA protein quantification kit	Nanjing Jiancheng Bioengineering Institute	Cat#: A045-4-2
BCA protein quantification kit	Beyotime Biotechnology	Cat#: P0010S
Extracellular OCR Plate Assay Kit	Dojindo	Cat#: E297
Click EdU-488 cell proliferation kit	Shenzhen Zike Biotechnology	Cat#: ZK-PL4013
C2C12 medium	Wuhan Pricella Biotechnology	Cat#: CM-0044
MUSCs medium	Wuhan Pricella Biotechnology	Cat#: CM-M206
Deposited data		
Metagenomic sequencing data	This paper	PRJNA961984
Metabolomic sequencing data	This paper	MTBLS7752
Raw data and uncropped scans of Western blots	This paper	Data S1. All datasets generated in this study can be obtained from the lead contact.
Experimental models: Cell lines		
C2C12 cells	Wuhan Pricella Biotechnology	Cat#: CL-0044
Mouse Skeletal Muscle Stem Cells	Wuhan Pricella Biotechnology	Cat#: CP-M206
Experimental models: Organisms/strains		
SPF C57BL/6 mice	Guangzhou Huatong Biological Technology Co., Ltd.	NA
Software and algorithms		
R (v3.6.3 and v4.2.1)	R project	https://www.r-project.org
GraphPad (v8.0)	N/A	https://www.graphpad.com
Cytoscape (v3.6.1)	Shannon et al. ⁹⁶	N/A
HUMAnN3 (v3.7)	Beghini et al. ⁹⁷	https://huttenhower.sph.harvard.edu/humann
MetaPhiAn3 (v3.0.14)	Beghini et al. ⁹⁷	https://huttenhower.sph.harvard.edu/metaphian3

EXPERIMENTAL MODEL AND STUDY PARTICIPANT DETAILS

Participant recruitment

Altogether 43 individuals diagnosed with sarcopenia and 37 matched healthy individuals were enrolled. All individuals were recruited from Hainan General Hospital. All participants in this study were from Renhe Village, Longtang Town, Haikou City, Hainan Province, and were recruited and samples were collected by doctors from Hainan General Hospital. Being from the same village (community), the living environment, living conditions and assisted living facilities were similar for all Participants. Each participant provided written informed consent.

According to Asian Working Group for Sarcopenia, the inclusion criteria for sarcopenia were as follows.

- (1) grip strength thresholds <28 kg for males and <18 kg for females.
- (2) ASM thresholds: <7.0 kg/m² for males and <5.7 kg/m² for females.
- (3) Physical function threshold: FTCS ≥ 12 s.
- (4) Age ≥ 60 years, no sex restrictions. Participants must voluntarily sign an informed consent form.

The exclusion criteria were as follows.

- (1) Suffers from a variety of acute or chronic infections, immune disorders, or organ failure diseases, such as end-stage renal disease, liver failure, heart failure, and respiratory failure.
- (2) Individuals with endocrine disorders such as thyroid dysfunction, Cushing's syndrome, and pituitary dysfunction.
- (3) Participants who used antibiotics or probiotic preparations within one month prior to the study, or who had a history of diarrhea or gastroenteritis within two weeks.
- (4) Participants who are required to take medications for osteoporosis, corticosteroids, thyroid hormones, sex hormones, or acid secretion inhibitors.
- (5) Participants with a long history of alcohol consumption, defined as drinking for more than five years or ethanol intake exceeding 140 g/week for males and 70 g/week for females. Participants were divided into two groups based on the inclusion and exclusion criteria outlined above. Individuals diagnosed with sarcopenia were classified into the sarcopenia group, while those who did not meet the diagnostic criteria were classified into the healthy control group. The ancestry and gender of the participants were not documented. Details regarding the human subjects, including age, sex, race, and ethnicity, are provided in [Table S1](#).

The sample size was determined based on a prior power analysis to ensure the statistical power and robustness of the study results. Specifically, we used the expected effect size, an α level of 0.05, and a statistical power of 80% as the basis for the calculation, ultimately determining the minimum sample size required per group. The present study followed the principles of the Declaration of Helsinki. The Ethics Committee of Hainan General Hospital approved the study (Yi Lunyan (2022) No. 511). The full clinical trial registration is available at the Chinese Clinical Trial Registry (<https://www.chictr.org.cn>, ChiCTR2300073891).

Bacterial culture

B. adolescentis ATCC15703 was obtained from the Guangdong Microbial Culture Collection Center. *B. adolescentis* was cultured anaerobically in TPY medium at 37°C. Bacterial cells were harvested by centrifugation at 3200 rpm for 4 min. Subsequently, the cells were resuspended in sterile PBS to obtain a suspension with a density of 5×10^8 CFU per 200 μ L. Freshly prepared bacterial suspensions were used for daily gavage in animal experiments.

Animal experiments

Male wild-type C57BL/6J young (9 weeks old) and aged (18 months old, approximately equivalent to 56–69 years in humans) mice were obtained from Guangzhou Huatong Biological Technology Co., Ltd. (Guangdong, China). All procedures involving experimental animals were conducted in accordance with protocols approved by the Animal Research Committee of Hainan University and complied with the Guide for the Care and Use of Laboratory Animals (Ethics No. HNUAUCC-2024-00256 and HNUAUCC-2024-00257). All animals were housed under specific pathogen-free conditions in standard facilities with controlled temperature and humidity and had *ad libitum* access to food and water. During the experiment, the mice were free to use the same water and feed. In both animal experiments, the Young group ($n = 8$) and the Aged group ($n = 8$) were administered equal amounts of PBS daily by oral gavage. The *B. adolescentis* group ($n = 8$) received 5×10^8 CFU per 200 μ L of *B. adolescentis* daily by oral gavage for five consecutive weeks. The nicotinic acid group ($n = 8$) received 150 mg/kg of nicotinic acid per 200 μ L daily by oral gavage for five consecutive weeks. Nicotinic acid (Aladdin Biochemical Technology, China) was freshly prepared daily and dissolved in sterile PBS. The dosage of 150 mg/kg was calculated based on the individual body weight of each mouse to ensure accuracy. The solution was prepared immediately before administration to maintain stability and efficacy. Mice were continuously gavaged with 150 mg/kg of nicotinic acid daily for a duration of five weeks. We used a computer-generated randomization list to assign animals to different groups, ensuring randomness and balance within groups. To avoid potential bias, all researchers involved in data collection and analysis were strictly blinded to the treatment group information throughout the experiment. The sample size calculation was based on *a priori* power analysis to ensure statistical power and robustness of the study results. The calculation was performed using the expected effect size, α level (0.05), and statistical power (80%), ultimately determining the minimum sample size required per group.

To minimize selection bias and ensure balance in group allocation, we used a computer-generated randomization list to assign animals to different treatment groups. Specifically, each animal was randomly assigned to an experimental group or a control group using a random number generator at the time of grouping, ensuring randomness and balance within the groups. To avoid potential bias, all researchers involved in data collection and analysis were blinded to the treatment group information throughout the experiment. Specifically, animal treatment group labels were encoded by an independent party prior to the experiment, so researchers were unable to directly access group information. During the data analysis phase, a different research team was responsible for unblinding the data, ensuring that data processing was free from any human bias. This blinding procedure was applied consistently throughout the entire experiment, including behavioral observations, biochemical analysis, and tissue assessments.

Cell culture assay

The C2C12 cells and MUSCs were purchased from Wuhan Pricella Biotechnology Co., Ltd., China (Cat No.: CL-0044 and CP-M206). The C2C12 myoblast cell lines were authenticated through STR profiling, while MUSCs were isolated from mouse skeletal muscle

tissue and verified for identity and purity using Desmin immunofluorescence staining. Both C2C12 and MUSCs were tested negative for mycoplasma contamination. C2C12 cells were cultured in specific C2C12 medium (Cat No.: CM-0044, containing 10% fetal bovine serum, 1% penicillin/streptomycin in DMEM) at 37°C with 5% CO₂. When the cells reached approximately 80% confluence, differentiation was induced by changing the medium to differentiation medium (high-glucose DMEM +2% horse serum +1% P/S). Logarithmic-phase C2C12 cells were seeded at 2.5 × 10⁴ cells per well in a culture dish and cultured overnight at 37°C with 5% CO₂ incubator to allow cell attachment. Nicotinic acid was dissolved to a final concentration of 0.75 mM in complete medium after being weighed, sonicated for 10 min, and filtered through a 0.22 µm filter. Dexamethasone was weighed and dissolved in DMSO to a final concentration of 100 mM, then diluted to 10 µM in complete medium.⁵⁰ C2C12 cells were divided into three groups: control group (Con, complete medium), dexamethasone group (Dex, 10 µM), and nicotinic acid group (Dex+NA, 10 µM dexamethasone +0.75 mM nicotinic acid). After 24 h of treatment, the medium was removed, cells were washed with PBS, digested with trypsin, washed twice with PBS, and collected for NAD+ level and RNA extraction.

MUSCs were cultured in specific MUSCs medium (Cat No.: CM-M206, containing 10% FBS, 10% horse serum, 1% penicillin/streptomycin, epidermal growth factor, and basic fibroblast growth factor in DMEM) at 37°C with 5% CO₂.³⁶ Nicotinic acid was dissolved in complete medium to a final concentration of 0.75 mM after being weighed, sonicated for 10 min, and filtered through a 0.22 µm filter.

Logarithmic-phase MUSCs were counted, and the cell concentration was adjusted to 9 × 10⁴ cells per well, seeded in 6 cm dishes, and cultured overnight at 37°C with 5% CO₂ to allow cell attachment. MUSCs were divided into two groups: control group (Con, complete medium) and nicotinic acid group (NA, nicotinic acid dissolved in complete medium). After 48 h of treatment, cells were counted. The medium was removed, cells were washed twice with PBS, digested with trypsin, washed twice with PBS, and collected for NAD+ content measurement.

METHOD DETAILS

Human biosample collection

Trained personnel measured the subjects' height, weight, and calf circumference. Measurement of the grip strength of the subject's dominant hand using a calibrated dynamometer (CAMRY EH101, China) while the subjects were seated. A bioelectrical impedance analyzer (Runcobo CP10A, China) was used to measure the ASM of the subjects. Physical function was assessed using the 5TCS. Blood samples were collected from the subjects after a 10-h fast and analyzed immediately. Serum samples were separated for metabolomics. Fecal samples were collected and treated with a preservative (CW0592M, CWBIO) to stabilize nucleotides for shotgun metagenomics.

Fecal shotgun metagenomic sequencing

Fecal metagenomic DNA was extracted using the QIAamp Fecal DNA Mini Kit (Qiagen, Germany). Subsequently, DNA quality was examined using agarose gel electrophoresis.⁹⁸ After determining the DNA concentration, libraries were constructed and sequenced on the NovaSeq 6000 platform (Illumina, USA) to generate 150 bp paired-end reads. Quality control measures were applied to the raw sequencing reads. Low-quality bases were trimmed, and adapter sequences were removed using the FastQC tool. Reads that mapped to the host genome were filtered out, and only microbial reads were retained.⁹⁹ We applied the Total Sum Scaling (TSS) normalization method to ensure comparability across samples.

Metagenomic species identification and functional annotation

Species annotation was performed using Humann software (v3.7). Differential gut species were screened using the Mann-Whitney test. The metabolic pathway functional profiles of the identified species were obtained based on the MetaCyc database.¹⁰⁰ The functional annotations of metagenomic samples were regrouped using the humann_regroup_table command based on the KEGG database.

Selection of microbial species associated with sarcopenia

To calculate the differences in gut microbiome richness and structure among subjects, the "vegan" package was used to compute the α -diversity and similarity between samples. Principal coordinates analysis (PCoA) was conducted based on Bray-Curtis distances. The Spearman rank correlation coefficient (R value) between each metric and differential species was calculated using the cor function, and the significance of the correlation (p -value) was determined using the corPvalueStudent function. To eliminate the impact of age on muscle function indices (ASMI, grip strength, calf girth, and 5TCS), we first performed linear regression analysis for each index against age and extracted the residuals as adjusted values. Then, we used Spearman correlation analysis to calculate the correlation coefficients between bacterial abundances and these adjusted indices. The significance of these correlations was evaluated by computing the p -values. A random forest model was constructed using the "RandomForest" R package, with subjects' samples randomly split into training and validation sets at a 1:1 ratio.¹⁰¹ This model was used to determine the importance of each key species in distinguishing sarcopenic subjects from normal controls.

Serum untargeted metabolomics analysis

Serum samples were collected from subjects and mixed with an extraction solution containing internal standards (acetonitrile = 1:4, V/V). The internal standards used were 2-chlorophenylalanine, L-phenylalanine (2-13C), [2H4]-melatonin, [2H4]-succinic

acid, 4-fluoro-L-phenylglycine, lidocaine, and deuterated testosterone. An appropriate amount of the filtrate was retained for subsequent separation. The chromatographic separation was carried out on a Waters ACQUITY UPLC HSS T3 C18 1.8 μ m column using the UPLC system.¹⁰² The column temperature was at 40°C, with a flow rate of 0.4 mL/min and an injection volume of 2 μ L. The raw LC-MS data were transformed to mzML format, and baseline correction and peak alignment were performed using ProteoWizard software. After correction and screening, metabolite identification information was obtained based on databases (Maeve Metabolomics Laboratory, <http://www.metware.cn/>; and HMDB, <http://www.hmdb.ca/>).¹⁰³ The gradient program of UPLC is as follows: 0 min 95:5 V/V, 11.0 min 10:90 V/V, 12.0 min 10:90 V/V, 12.1 min 95:5 V/V, and 14.0 min 95:5 V/V. The conditions for mass spectrometry analysis are as follows: The data acquisition duration was 14 min. The IonSpray voltage was set to 5500 V in positive ion mode and -4500 V in negative ion mode. The Electrospray Ionization (ESI) temperature was maintained at 550°C in positive ion mode and 450°C in negative ion mode. The Ion Source Gas1 (spray gas) pressure was set to 50 psi for both modes, and the Ion Source Gas2 pressure was set to 60 psi for both modes. The Curtain Gas (CUR) pressure was set to 35 psi. The declustering potential was set to 60 V in positive ion mode and -60 V in negative ion mode. The MS1 collision energy was set to 10 V in positive ion mode and -10 V in negative ion mode, while the MS2 collision energy was set to 30 V in positive ion mode and -30 V in negative ion mode.

Nicotinic acid quantification

Detailed mass spectrometry settings included: Electrospray Ionization (ESI) temperature at 550°C, mass spectrometer voltage at 5500 V in positive ion mode and -4500 V in negative ion mode, and curtain gas at 35 psi. In the Q-Trap 6500+ system, each ion pair was scanned and detected based on optimized declustering potential and collision energy. Mass spectrometry data were processed using Analyst 1.6.3 software. Quantification was performed using a triple quadrupole mass spectrometer's Multiple Reaction Monitoring mode.

Selection of microbial functions and metabolites associated with *B. adolescentis*

First, the metabolomics data's principal component analysis (PCA) was performed using the "prcomp" R function and "ggplot2" R package. Differential serum metabolites between sarcopenic subjects and normal controls were calculated using the Student's T test. We applied the Benjamini-Hochberg method for false discovery rate (FDR) correction to the differential metabolites in the metabolomics data, using the p.adjust function in R. After correction, metabolites with FDR-adjusted *p*-values <0.05 were considered to exhibit significant differences. Subsequently, metabolites significantly correlated with both *B. adolescentis* and clinical indicators were screened based on correlation methods. Metabolite enrichment analysis was performed based on MetaboAnalyst (<https://www.metaboanalyst.ca>). The random forest model was employed to identify important metabolites differentiating sarcopenic subjects from normal controls. Constructing a linear model using the "lm" R function. The association between nicotinic acid and various muscle indicators was calculated using linear models. Finally, the NCBI database and MetOrigin database (<https://metorigin.met-bioinformatics.cn>)¹⁰⁴ were used to trace the origin of metabolites, confirming the nicotinic acid-producing capability of *B. adolescentis*.

Grip strength measurement in mice

Mice were allowed to acclimate in the behavioral laboratory for 10 min before each experiment, with temperature and light conditions kept consistent for all mice.¹⁰⁵ The grip strength was assessed using a digital force gauge (Puyan DS2-50N, China) connected to a metal grid. Mice were placed on a line parallel to the grid, and their tails were gently pulled backward in a horizontal direction parallel to the force gauge until the mice could no longer resist the applied force. Peak force was recorded in grams. Each measurement was repeated four times, with a 5-min interval between each measurement.¹⁰⁶

Treadmill task

Before the formal running test, mice underwent a warm-up training session on a treadmill at the lowest speed without an incline. Subsequently, the treadmill's incline and speed were gradually increased until the mice could no longer run and were removed from the treadmill. The distance covered and the time to exhaustion were recorded as the maximum running distance and time.¹⁰⁷

Histology

Skeletal muscles were collected from mice and weighed, with some portions fixed in 4% paraformaldehyde and others snap-frozen in liquid nitrogen and stored at -80°C. The fixed muscle tissues were embedded in paraffin, sectioned, and analyzed using antibody staining. Antibodies used included anti-PAX7 (PAX7 rabbit polyclonal, Servicebio, China), anti-dystrophin (Dystrophin rabbit polyclonal antibody, Servicebio, China), anti-COX IV antibody (Cytochrome c oxidase subunit 4 isoform 1, mitochondrial, Servicebio, China), anti-laminin antibody (Laminin antibody produced in rabbit, Sigma-Aldrich, USA), anti-MYH4 antibody (MYH4-Specific Polyclonal antibody, Poteintech, China), and anti-MYH7 antibody (Slow skeletal myosin heavy chain mouse mAb, Servicebio, China). After primary antibody incubation, sections were incubated with appropriate secondary antibodies for 50 min in the dark. Subsequently, nuclei were counterstained with DAPI (DAPI staining reagent, Servicebio, China). Images were captured after mounting, and the integrated fluorescence signal of each image was calculated using ImageJ software (v1.54g) with consistent threshold and image size settings.

Quantitative determination of nicotinic acid

Samples were spiked with 250 μ L of methanol solution containing 10 μ L of 250 ng/mL internal standard working solution.¹⁰⁸ The column was a Waters ACQUITY UPLC HSS T3 C18 at a flow rate of 0.35 mL/min and a column temperature of 40°C. Mobile phase A was ultrapure water containing 0.1% formic acid, and mobile phase B was acetonitrile containing 0.1% formic acid. Detailed mass spectrometry settings were provided in Supplementary materials. Integration and quantification of chromatographic peaks of all target compounds using standard curves.¹⁰²

NAD⁺ measurement

The levels of NAD⁺ in muscle tissue, cell, and serum samples were measured using NAD⁺/NADH assay kits from Biovision (Beyotime Biotechnology, China) and Nanjing Jiancheng Bioengineering Institute (China). The NAD⁺ levels in muscle tissue and cell samples were normalized to the protein levels of the samples.

ATP content measurement

The ATP content in mouse skeletal muscle was measured using an ATP assay kit from Nanjing Jiancheng Bioengineering Institute. The ATP contents were normalized to the protein levels of the samples.

Gene expression analysis by real-time quantitative RT-PCR

Total RNA was extracted from muscle tissue and cells using TRIzol reagent. Reverse transcription was performed using the RevertAid First Strand cDNA Synthesis Kit (Thermo Fisher Scientific, USA). The synthesized cDNA was mixed with SYBR qPCR Mix and subjected to quantitative real-time PCR on a fluorescence detection system (Jena, Germany) to quantify the expression of target genes. Data were normalized to GAPDH. Table S2 provides details of the gene-specific primers.

Mitochondrial DNA copy number quantification

The relative copy number of mtDNA to nuclear DNA in muscle tissue was determined by qPCR.⁵⁰

Citrate synthase activity measurement

The activity level of citrate synthase in muscle tissue was measured using the citrate synthase (CS) assay kit from Nanjing Jiancheng Bioengineering Institute. The results were normalized to the protein levels of the samples.

Measurement of mitochondrial complex I and complex II

The activities of mitochondrial complex I and complex II were measured using mitochondrial respiratory chain complex I and complex II activity assay kits from Solarbio (Solarbio, China). The results were normalized to the protein levels of the samples.

Measurement of cellular OCR

OCR was measured using the Extracellular OCR Plate Assay Kit (E297, Dojindo, Kumamoto, Japan) according to the manufacturer's protocol. Briefly, C2C12 cells (8×10^4 cells) were seeded overnight in a 96-well black plate. Cells were treated with the oxygen probe in the assay medium (RB) and incubated at 37°C for 30 min. Cells were then stimulated with 10 μ M dexamethasone and 10 μ M dexamethasone +0.75 mM nicotinic acid, and mineral oil was added. Fluorescence intensity was recorded every 10 min using a microplate reader (excitation wavelength of 500 nm, emission wavelength of 650 nm). OCR was calculated by analyzing the dynamic profile of the measurements.¹⁰⁹

EdU assay for detection of proliferation in MUSCs

MUSCs at the logarithmic growth phase were seeded at a density of 8×10^4 cells per dish in confocal-specific culture dishes. The cells were cultured overnight in a 37°C, 5% CO₂ incubator to allow adhesion. After 48 h of nicotinic acid treatment, cell proliferation was assessed using the Click EdU-488 cell proliferation detection kit (ZK-PL4013, China) according to the manufacturer's instructions. Finally, the ratio of EdU-positive cells to total cells (DAPI-stained) was calculated using ImageJ software.

Western blot analysis

Tissues were lysed and mixed with will protein solution and loading buffer and denatured at 95°C for 10 min. The samples were subjected to SDS-PAGE electrophoresis, then transferred to a PVDF membrane. After blocking the membrane with 5% skimmed milk for 30 min, the primary antibody was incubated overnight at 4°C on a shaker, and finally the secondary antibody was incubated. ECL A and B solutions were mixed at a 1:1 ratio, and the membrane was immersed in the solution for 1 min. The chemiluminescence signal was detected using an imaging system, and images were saved and analyzed.

QUANTIFICATION AND STATISTICAL ANALYSIS

Boxplots were generated using the "ggplot2" R package. Species differences were displayed using the "pheatmap" R package. Histograms were created using GraphPad 8.0, with values expressed as mean \pm SEM. Correlation networks were drawn using

Cytoscape software. To ensure the validity of parameter tests, we conducted normality tests on the data prior to all statistical analyses. When the data did not meet normality assumptions, we applied non-parametric tests such as the Kruskal-Wallis test or the Wilcoxon rank-sum test. For PCA and PCoA, the significance of group differences was evaluated using the Anosim and Adonis test. The significance levels indicated as * $p < 0.05$, ** $p < 0.01$, *** $p < 0.001$.

ADDITIONAL RESOURCES

The full clinical trial registration is available at the Chinese Clinical Trial Registry (<https://www.chictr.org.cn>, ChiCTR2300073891).